

---

# IMEX–RB: A SELF–ADAPTIVE IMPLICIT–EXPLICIT TIME INTEGRATION SCHEME EXPLOITING THE REDUCED BASIS METHOD

---

Micol Bassanini<sup>1</sup>   Simone Deparis   Francesco Sala   Riccardo Tenderini

*Institute of Mathematics, EPFL, Lausanne, Switzerland*

## ABSTRACT

In this work, we introduce a self–adaptive implicit–explicit (IMEX) time integration scheme, named IMEX–RB, for the numerical integration of systems of ordinary differential equations (ODEs), arising from spatial discretizations of partial differential equations (PDEs) by finite difference methods. Leveraging the Reduced Basis (RB) method, at each timestep we project the high–fidelity problem onto a suitable low–dimensional subspace and integrate its dynamics implicitly. Following the IMEX paradigm, the resulting solution then serves as an educated guess within a full–order explicit step. Notably, compared to the canonical RB method, IMEX–RB neither requires a parametrization of the underlying PDE nor features an offline–online splitting, since the reduced subspace is built dynamically, exploiting the high–fidelity solution history. We present the first–order formulation of IMEX–RB, demonstrating and showcasing its convergence and stability properties. In particular, under appropriate conditions on the method’s hyperparameters, IMEX–RB is unconditionally stable. The theoretical analysis is corroborated by numerical experiments performed on representative model problems in two and three dimensions. The results demonstrate that our approach can outperform conventional time integration schemes like backward Euler. Indeed, IMEX–RB yields high–fidelity accurate solutions, provided that its main hyperparameters — namely the reduced basis size and the stability tolerance — are suitably tuned. Moreover, IMEX–RB realizes computational gains over backward Euler for a range of timestep sizes above the forward Euler stability threshold.

**Keywords** Implicit–explicit time integration, reduced basis method, partial differential equations, finite differences

## 1 Introduction

Stability is a critical aspect when applying time–marching schemes to stiff dynamical systems, namely systems characterized by widely varying timescales and whose numerical integration is therefore challenging. In this work, we specifically focus on ordinary differential equations (ODEs) that stem from spatial discretizations of partial differential equations (PDEs) by finite difference schemes.

Explicit time integration methods, such as forward Euler, may represent an attractive choice for many problems, since they entail little computational cost and feature relatively straightforward implementations. However, for stiff systems, their use becomes impractical due to strict stability constraints that require choosing very small timestep sizes [1, 2, 3]. Nonetheless, these constraints are dictated by the fastest timescales, which may not be relevant to the physical phenomena of interest and may arise from transient and/or numerically induced effects [4]. As a result, explicit methods often lead to overly accurate solutions, thereby involving excessively large computational costs.

Implicit methods, such as backward Euler, offer superior stability properties compared to explicit schemes, hence allowing the use of larger timesteps. Therefore, they are generally more suitable for the numerical approximation of stiff dynamical systems. Although they require solving a system of equations — possibly nonlinear — at each time step, which inevitably entails larger computational costs and implementation efforts. As a result, implicit schemes trade larger complexity for enhanced stability [5].

---

<sup>1</sup>Corresponding author: Email: [micol.bassanini@epfl.ch](mailto:micol.bassanini@epfl.ch)

In this scenario, hybrid methods, called Implicit–Explicit (IMEX), have been designed [6, 7]. In essence, IMEX methods aim at combining the advantages of explicit and implicit schemes, featuring remarkable stability properties and convenient costs. A relevant example is represented by additive and partitioned Runge–Kutta methods [8, 9]. By integrating stiff terms implicitly and non–stiff terms explicitly, these schemes achieve superior efficiency compared to their explicit counterparts, relaxing timestep size constraints [9]. However, their performance heavily depends on how the system is partitioned, which requires *a priori* knowledge of the underlying physics. In particular, their design is challenging for complex systems, characterised by a large number of equations and variables, such as two–fluid turbulence plasma model [10] or gyrokinetic simulations [11]. Indeed, in these scenarios, the interactions between different physical processes, and specifically the interplay of fast and slow dynamics, make it difficult to distinguish terms based on their stiffness.

An alternative splitting technique, often associated with exponential methods, is *dynamic linearization*, also known as *Jacobian splitting* [12]. Notably, this approach does not require any prior knowledge of the problem’s physics. By adding and subtracting the right–hand side operator Jacobian, dynamic linearization partitions into a stiff linear term, given by the right–hand side Jacobian evaluated at the most recent timestep, and a convenient Lipschitz–continuous nonlinear term, characterized by a small Lipschitz constant. Then, the latter is integrated explicitly, while the former, being stiff, is treated implicitly [13]. Albeit showcasing remarkable performances, we note that this approach nonetheless entails a high–fidelity implicit step and so non–negligible computational costs.

To circumvent the issues related to physics–based splitting, while at the same time retaining the stability properties of IMEX schemes, in this work we present a novel self–adaptive IMEX time integrator, named IMEX–RB. Remarkably, the splitting strategy underlying IMEX–RB does not require any prior knowledge of the problem physics nor of its spectral properties; furthermore, the splitting is self–adaptive as it is dynamically updated as time integration proceeds. Ultimately, the proposed scheme balances efficiency and robustness, offering high–fidelity accurate solution approximations at convenient computational costs, lower than those of conventional implicit methods for a wide range of timestep sizes.

The workhorse of IMEX–RB is the Reduced Basis (RB) method [14, 15], the most popular example of projection–based reduced order model (ROM). Compared to traditional high–fidelity models, the main idea of ROMs is to deliver precise enough solution approximations, whose quality actually depends on the task at hand, while drastically lowering the computational costs. Projection–based ROMs, in particular, achieve this goal by projecting the full–order problem, namely the one stemming from the spatial or spatio–temporal discretization of the PDE at hand, onto a suitably defined low–dimensional subspace, where the dynamics are evolved. This approach is particularly convenient when dealing with parametrized PDEs, i.e. PDEs that depend on one or more parameters, such as physical properties (e.g. density, viscosity) or geometrical features. Indeed, in this context, the solution manifold is inherently finite–dimensional and it can be approximated exploiting *a priori* knowledge of a select number of snapshots and of the corresponding parameter values. Specifically, the manifold is approximated by a low–dimensional linear subspace, spanned by basis functions that are typically computed through Proper Orthogonal Decomposition [16, 17] or greedy approaches [18, 19]. In recent years, significant progress has been made in designing RB methods for time–dependent nonlinear problems that are accurate, efficient, and stable [20, 21, 22, 23, 24]. It is worth remarking that the effectiveness of RB depends on how precisely the PDE solution manifold can be fitted into a low–dimensional linear subspace, which can be expressed through the Kolmogorov  $n$ –width [25]. In this regard, many problems, such as advection–dominated systems, wave–like equations and conservation laws, are well–known to feature large Kolmogorov  $n$ –widths and thus represent common pitfalls for the RB method.

Recently, major effort has also been devoted to the implementation of methods that leverage low–rank structures, commonly found in high–dimensional PDE solutions, to accelerate computations while preserving the accuracy, stability, and robustness of classical approaches. Popular examples in this regard are represented by the Dynamical Low Rank (DLR) approximation [26] and by Step–and–Truncation (SAT) methods, [27]. For instance, within the DLR framework, several robust and accurate time integration techniques have been developed, including Projection DLR methods [28] and the Basis Updating and Galerkin (BUG) integrator [29]. By analogy with the IMEX–RB method, both the augmented BUG [30] and the Reduced Augmentation Implicit Low–rank (RAIL) [31] scheme dynamically update a low–dimensional basis over time.

In a nutshell, IMEX–RB operates in two stages. In the first stage, the RB method is employed to approximate the solution efficiently; notably, the small dimension of the reduced problem enables implicit time integration at a negligible computational cost. In the second stage, the prediction obtained from the reduced system is leveraged as an educated guess within a full–order explicit step, obeying the IMEX paradigm. The reduced subspace is generated through QR decomposition of the recent solution history matrix, and it is therefore dynamically updated over time. Furthermore, the reduced basis is suitably enriched at each timestep to guarantee absolute stability. Unlike conventional DLR time integration methods, IMEX–RB does not assume that the solution is inherently low–rank. Rather,

our approach adaptively augments the reduced subspace so that it approximately contains the solution at the current timestep.

The paper is organized as follows. Section 2 presents the first–order IMEX–RB method, as resulting from the combination of the forward and backward Euler schemes, and demonstrates its convergence and absolute stability. Moreover, the complexity of the proposed algorithm is discussed and compared with that of backward Euler. In Section 3, the performance of the method is empirically evaluated on three different numerical experiments. Specifically, we use IMEX–RB to solve a 2D advection–diffusion equation, a 2D viscous Burgers’ equation, and a 3D advection–diffusion equation. Finally, in Section 4 we draw the conclusions, we list the main limitations and we discuss possible further developments.

## 2 Methods

In this section, we provide a detailed description of the proposed IMEX–RB method, as resulting from the convenient combination of a reduced backward Euler scheme and a high-fidelity explicit step. We initially describe the structure of IMEX–RB, highlighting its more relevant features. Subsequently, we demonstrate that, under suitable hypotheses, the proposed method is first–order convergent and absolutely stable. Finally, we report the complete algorithm with a few considerations on the associated computational costs and memory requirements.

### 2.1 Problem setup

We consider systems of ODEs that typically arise from the semi–discretization in space of PDEs by finite difference methods. In particular, we consider the following Cauchy problem:

find  $\mathbf{y} : I \subset \mathbb{R} \rightarrow \mathbb{R}^{N_h}$ ,  $\mathbf{y} \in C^2(I)$ , such that

$$\begin{cases} \mathbf{y}'(t) = \mathbf{f}(t, \mathbf{y}(t)), & \forall t \in I \\ \mathbf{y}(0) = \mathbf{y}_0, \end{cases} \quad (1)$$

where  $I = (0, T]$  is the time interval,  $\mathbf{f} : I \times \mathbb{R}^{N_h} \rightarrow \mathbb{R}^{N_h}$  is a known function and  $\mathbf{y}'$  is the first derivative of  $\mathbf{y}$  with respect to  $t$ . Moreover,  $\mathbf{y}_0 \in \mathbb{R}^{N_h}$  is the initial condition. Here  $N_h \in \mathbb{N}$  denotes the number of degrees of freedom (DOFs), stemming from the discretization in space of the underlying PDE. The problem in Eq. (1) is well–posed if  $\mathbf{f}$  is bounded, continuous in both arguments, and Lipschitz continuous in its second argument. These assumptions are understood in the following derivation; we further denote by  $L > 0$  the Lipschitz constant of  $\mathbf{f}$ .

### 2.2 The IMEX–RB method

For a given  $N_t \in \mathbb{N}$ , we build a sequence  $\{\mathbf{u}_n\}_{n=0}^{N_t}$  approximating  $\mathbf{y}(t_n)$ ,  $n = 0, \dots, N_t$ , where  $t_n = n\Delta t$  and  $\Delta t := T/N_t$  is the timestep, i.e. we assume  $t_0 = 0$  for simplicity.

The proposed IMEX–RB scheme allows for a stable and efficient numerical integration of ODEs systems by exploiting two steps. In the first one, a backward Euler step is projected onto a conveniently defined reduced subspace  $\mathcal{V}_n$  of dimension  $N \ll N_h$ , spanned by the orthonormal columns of a matrix  $\mathbf{V}_n \in \mathbb{R}^{N_h \times N}$ , whose assembly is the subject of Section 2.5. In the second step, instead, we explicitly integrate Eq. (1) through a modified forward Euler step, employing the available intermediate RB solution as a convenient evaluation point for  $\mathbf{f}$ . Formally, let  $\mathbf{u}_n \in \mathbb{R}^{N_h}$  be the approximate solution to Eq. (1) at time  $t_n$  computed with IMEX–RB. Also, let the reduced subspace be such that  $\mathbf{u}_n \in \mathcal{V}_n$ . Let  $\mathbf{u}_0 = \mathbf{y}(0)$ ; then, for  $n = 0, 1, \dots, N_t - 1$ , we compute  $\mathbf{u}_{n+1}$  as follows:

1. Solve a projected backward Euler step in the reduced space, looking for  $\delta \mathbf{u}_{n+1}^N \in \mathbb{R}^N$ ,

$$\delta \mathbf{u}_{n+1}^N = \Delta t \mathbf{V}_n^T \mathbf{f}(t_{n+1}, \mathbf{V}_n \delta \mathbf{u}_{n+1}^N + \mathbf{u}_n); \quad (2)$$

2. Compute  $\mathbf{u}_{n+1}$  explicitly, by conveniently exploiting the solution to Eq. (2):

$$\mathbf{u}_{n+1} = \mathbf{u}_n + \Delta t \mathbf{f}(t_{n+1}, \mathbf{V}_n \delta \mathbf{u}_{n+1}^N + \mathbf{u}_n). \quad (3)$$

In the following derivations, we assume that  $\mathbf{u}_n \in \mathcal{V}_n$ . Additional details about the definition and construction of the subspace  $\mathcal{V}_n$  are discussed in Section 2.5.

**Lemma 2.1.** *The scheme represented by Eqs. (2)–(3) can be equivalently written in the form:*

$$\mathbf{u}_{n+1} = \mathbf{u}_n + \Delta t \mathbf{f}(t_{n+1}, \mathbf{V}_n \mathbf{V}_n^T \mathbf{u}_{n+1}). \quad (4)$$

*Proof.* On the one hand, since  $\mathbf{u}_n \in \mathcal{V}_n$ , it follows that  $\mathbf{u}_n = \mathbf{V}_n \mathbf{V}_n^T \mathbf{u}_n$ , and thus projecting Eq. (3) onto the subspace  $\mathcal{V}_n$  yields:

$$\mathbf{V}_n \mathbf{V}_n^T \mathbf{u}_{n+1} = \mathbf{u}_n + \Delta t \mathbf{V}_n \mathbf{V}_n^T \mathbf{f}(t_{n+1}, \mathbf{V}_n \delta \mathbf{u}_{n+1}^N + \mathbf{u}_n).$$

On the other hand, the reduced coefficients  $\delta \mathbf{u}_{n+1}^N \in \mathbb{R}^N$  satisfy the backward Euler step of Eq. (2). Pre–multiplying by  $\mathbf{V}_n$  and adding  $\mathbf{u}_n$  on both sides yields:

$$\mathbf{V}_n \delta \mathbf{u}_{n+1}^N + \mathbf{u}_n = \mathbf{u}_n + \Delta t \mathbf{V}_n \mathbf{V}_n^T \mathbf{f}(t_{n+1}, \mathbf{V}_n \delta \mathbf{u}_{n+1}^N + \mathbf{u}_n).$$

This confirms that  $\mathbf{V}_n \mathbf{V}_n^T \mathbf{u}_{n+1} = \mathbf{V}_n \delta \mathbf{u}_{n+1}^N + \mathbf{u}_n$ , thus showing that the right–hand sides of Eqs. (3) and (4) are equal. This proves Eq. (4).

Now, let Eq. (4) hold. Take

$$\delta \mathbf{u}_{n+1} := \mathbf{u}_{n+1} - \mathbf{u}_n = \Delta t \mathbf{f}(t_{n+1}, \mathbf{V}_n \mathbf{V}_n^T \mathbf{u}_{n+1}).$$

Then

$$\mathbf{V}_n^T \delta \mathbf{u}_{n+1} = \Delta t \mathbf{V}_n^T \mathbf{f}(t_{n+1}, \mathbf{V}_n \mathbf{V}_n^T \mathbf{u}_{n+1}),$$

and

$$\mathbf{V}_n \mathbf{V}_n^T \mathbf{u}_{n+1} = \mathbf{V}_n \mathbf{V}_n^T (\mathbf{u}_n + \delta \mathbf{u}_{n+1}) = \mathbf{u}_n + \mathbf{V}_n^T \delta \mathbf{u}_{n+1}.$$

Upon defining  $\delta \mathbf{u}_{n+1}^N := \mathbf{V}_n^T \delta \mathbf{u}_{n+1}$ , we obtain Eqs. (2) and (3).  $\square$

### 2.3 Convergence of IMEX–RB

First, we investigate the consistency of IMEX–RB.

**Proposition 2.2** (Consistency of IMEX–RB). *Consider the Cauchy problem of Eq. (1). Let  $\mathbf{y} \in C^2(I)$ , and suppose that  $\mathbf{f}$  is Lipschitz continuous in its second argument, with Lipschitz constant  $L > 0$ . Then, the IMEX–RB scheme is consistent of order 1.*

*Proof.* We proceed as in [32, p. 211]. Consider the equivalent reformulation of the IMEX–RB scheme in Eq. (4). Let  $\tau_{n+1}(\Delta t)$  be the local truncation error at time  $t_{n+1}$ . From its definition, and by imposing that the exact solution  $\mathbf{y}$  satisfies the scheme, we can write

$$\mathbf{y}(t_{n+1}) = \mathbf{y}(t_n) + \Delta t \mathbf{f}(t_{n+1}, \tilde{\mathbf{V}}_n \tilde{\mathbf{V}}_n^T \mathbf{y}(t_{n+1})) + \Delta t \tau_{n+1}(\Delta t), \quad (5)$$

where the notation  $\tilde{\mathbf{V}}_n$  accounts for the presence of the exact solution  $\mathbf{y}(t_n)$  inside the basis. A rearranged first-order Taylor expansion of  $\mathbf{y}(t_n)$  around  $t_{n+1}$  yields:

$$\mathbf{y}(t_{n+1}) = \mathbf{y}(t_n) + \Delta t \mathbf{f}(t_{n+1}, \mathbf{y}(t_{n+1})) - \frac{1}{2} \Delta t^2 \mathbf{y}''(\xi), \quad \xi \in [t_n, t_{n+1}]. \quad (6)$$

Subtracting Eq. (5) from Eq. (6) gives:

$$\tau_{n+1}(\Delta t) = \mathbf{f}(t_{n+1}, \mathbf{y}(t_{n+1})) - \mathbf{f}(t_{n+1}, \tilde{\mathbf{V}}_n \tilde{\mathbf{V}}_n^T \mathbf{y}(t_{n+1})) - \frac{1}{2} \Delta t \mathbf{y}''(\xi).$$

Taking the Euclidean norms and leveraging the Lipschitz continuity of  $\mathbf{f}$  in its second argument, we obtain:

$$\|\tau_{n+1}(\Delta t)\| \leq L \left\| \left( \mathbf{I} - \tilde{\mathbf{V}}_n \tilde{\mathbf{V}}_n^T \right) \mathbf{y}(t_{n+1}) \right\| + \frac{1}{2} \Delta t \|\mathbf{y}''(\xi)\|.$$

Since by hypothesis  $\mathbf{y}(t_n)$  lies in the range of  $\tilde{\mathbf{V}}_n$ , and thanks to Eq. (6), it holds that

$$\begin{aligned} \left( \mathbf{I} - \tilde{\mathbf{V}}_n \tilde{\mathbf{V}}_n^T \right) \mathbf{y}(t_{n+1}) &= \left( \mathbf{I} - \tilde{\mathbf{V}}_n \tilde{\mathbf{V}}_n^T \right) (\mathbf{y}(t_{n+1}) - \mathbf{y}(t_n)) \\ &= \Delta t \left( \mathbf{I} - \tilde{\mathbf{V}}_n \tilde{\mathbf{V}}_n^T \right) \mathbf{f}(t_{n+1}, \mathbf{y}(t_{n+1})) - \frac{1}{2} \Delta t^2 \left( \mathbf{I} - \tilde{\mathbf{V}}_n \tilde{\mathbf{V}}_n^T \right) \mathbf{y}''(\xi). \end{aligned}$$

Thus, the following estimate holds:

$$\|\tau_{n+1}(\Delta t)\| \leq \Delta t L \left\| \mathbf{f}(t_{n+1}, \mathbf{y}(t_{n+1})) \right\| + \frac{1}{2} \Delta t^2 L \|\mathbf{y}''(\xi)\| + \frac{1}{2} \Delta t \|\mathbf{y}''(\xi)\|.$$

Therefore, the global truncation error  $\tau(\Delta t) := \max_n \|\tau_{n+1}(\Delta t)\|$  satisfies:

$$\tau(\Delta t) \leq \Delta t L \max_{t \in I} \|\mathbf{y}'(t)\| + \frac{1}{2} (\Delta t + \Delta t^2 L) \max_{t \in I} \|\mathbf{y}''(t)\|.$$

Hence, since  $\mathbf{y} \in C^2(I)$ , we conclude that  $\tau(\Delta t) = \mathcal{O}(\Delta t)$ , and the IMEX–RB scheme is first-order consistent [33, p. 484].  $\square$

**Theorem 2.3** (Convergence of IMEX–RB). *Under the same assumptions of Proposition 2.2, the IMEX–RB method is convergent of order 1, i.e.  $\exists C > 0$  such that*

$$\|e_{n+1}\| := \|\mathbf{y}(t_{n+1}) - \mathbf{u}_{n+1}\| < C\Delta t.$$

*Proof.* We decompose the global error at  $t_{n+1}$  into two parts [33, p. 487]:

$$\mathbf{e}_{n+1} = (\mathbf{y}(t_{n+1}) - \mathbf{u}_{n+1}^*) + (\mathbf{u}_{n+1}^* - \mathbf{u}_{n+1}),$$

where

$$\mathbf{u}_{n+1}^* := \mathbf{y}(t_n) + \Delta t \mathbf{f}(t_{n+1}, \tilde{\mathbf{V}}_n \tilde{\mathbf{V}}_n^T \mathbf{y}(t_{n+1})).$$

Taking norms and using consistency gives

$$\|\mathbf{e}_{n+1}\| \leq \|\mathbf{y}(t_{n+1}) - \mathbf{u}_{n+1}^*\| + \|\mathbf{u}_{n+1}^* - \mathbf{u}_{n+1}\| \leq \Delta t \tau(\Delta t) + \|\mathbf{u}_{n+1}^* - \mathbf{u}_{n+1}\|. \quad (7)$$

We now bound the quantity  $\|\mathbf{u}_{n+1}^* - \mathbf{u}_{n+1}\|$ . First, we observe that

$$\mathbf{u}_{n+1}^* - \mathbf{u}_{n+1} = \mathbf{y}(t_n) - \mathbf{u}_n + \Delta t [\mathbf{f}(t_{n+1}, \tilde{\mathbf{V}}_n \tilde{\mathbf{V}}_n^T \mathbf{y}(t_{n+1})) - \mathbf{f}(t_{n+1}, \mathbf{V}_n \mathbf{V}_n^T \mathbf{u}_{n+1})].$$

By the Lipschitz continuity of  $\mathbf{f}$ , it follows that

$$\begin{aligned} \|\mathbf{u}_{n+1}^* - \mathbf{u}_{n+1}\| &\leq \|e_n\| + \Delta t \left\| \mathbf{f}(t_{n+1}, \tilde{\mathbf{V}}_n \tilde{\mathbf{V}}_n^T \mathbf{y}(t_{n+1})) - \mathbf{f}(t_{n+1}, \mathbf{V}_n \mathbf{V}_n^T \mathbf{u}_{n+1}) \right\| \\ &\leq \|e_n\| + \Delta t L \left\| \tilde{\mathbf{V}}_n \tilde{\mathbf{V}}_n^T \mathbf{y}(t_{n+1}) - \mathbf{V}_n \mathbf{V}_n^T \mathbf{u}_{n+1} \right\|. \end{aligned}$$

We assume  $\tilde{\mathbf{V}}_n$  is obtained by normalizing  $\mathbf{y}(t_n)$  and  $\mathbf{V}_n$  by normalizing  $\mathbf{u}_n$ ; hence,

$$\tilde{\mathbf{V}}_n := \frac{\mathbf{y}(t_n)}{\|\mathbf{y}(t_n)\|}, \quad \mathbf{V}_n := \frac{\mathbf{u}_n}{\|\mathbf{u}_n\|}.$$

The fallback when  $\|\mathbf{y}(t_n)\|$  is below a prescribed tolerance appears in Remark 2.4. We then write

$$\tilde{\mathbf{V}}_n \tilde{\mathbf{V}}_n^T \mathbf{y}(t_{n+1}) - \mathbf{V}_n \mathbf{V}_n^T \mathbf{u}_{n+1} = (\tilde{\mathbf{V}}_n \tilde{\mathbf{V}}_n^T - \mathbf{V}_n \mathbf{V}_n^T) \mathbf{y}(t_{n+1}) + \mathbf{V}_n \mathbf{V}_n^T (\mathbf{y}(t_{n+1}) - \mathbf{u}_{n+1}).$$

By the triangle inequality and since  $\left\| \tilde{\mathbf{V}}_n \tilde{\mathbf{V}}_n^T - \mathbf{V}_n \mathbf{V}_n^T \right\| = \left\| (\tilde{\mathbf{V}}_n - \mathbf{V}_n) \tilde{\mathbf{V}}_n^T + \mathbf{V}_n (\tilde{\mathbf{V}}_n - \mathbf{V}_n)^T \right\| \leq 2 \left\| \tilde{\mathbf{V}}_n - \mathbf{V}_n \right\|$ , we get

$$\left\| \tilde{\mathbf{V}}_n \tilde{\mathbf{V}}_n^T \mathbf{y}(t_{n+1}) - \mathbf{V}_n \mathbf{V}_n^T \mathbf{u}_{n+1} \right\| \leq 2 \left\| \tilde{\mathbf{V}}_n - \mathbf{V}_n \right\| \left( \|\mathbf{y}(t_{n+1})\| + \|\mathbf{u}_{n+1}\| \right). \quad (8)$$

Now, exploiting that, for two generic vectors  $\mathbf{a}, \mathbf{b} \in \mathbb{R}^K$ ,  $K \in \mathbb{N}$ , it holds

$$\left\| \frac{\mathbf{b}}{\|\mathbf{b}\|} - \frac{\mathbf{a}}{\|\mathbf{a}\|} \right\| \leq 2 \frac{\|\mathbf{b} - \mathbf{a}\|}{\|\mathbf{b}\|},$$

we obtain

$$\left\| \tilde{\mathbf{V}}_n - \mathbf{V}_n \right\| \leq 2 \frac{\|e_n\|}{\|\mathbf{y}_n\|}.$$

Substituting this result into Eq. (8) yields

$$\left\| \tilde{\mathbf{V}}_n \tilde{\mathbf{V}}_n^T \mathbf{y}(t_{n+1}) - \mathbf{V}_n \mathbf{V}_n^T \mathbf{u}_{n+1} \right\| \leq 4 \frac{\|\mathbf{y}(t_{n+1})\|}{\|\mathbf{y}(t_n)\|} \|e_n\| + \|e_{n+1}\|. \quad (9)$$

Hence, we have that

$$\|\mathbf{u}_{n+1}^* - \mathbf{u}_{n+1}\| \leq (1 + 4\Delta t CL) \|e_n\| + \Delta t L \|e_{n+1}\|, \quad (10)$$

where  $C = C(\Delta t) := \frac{\|\mathbf{y}(t_{n+1})\|}{\|\mathbf{y}(t_n)\|}$ , and  $C(\Delta t) \rightarrow 1$  as  $\Delta t \rightarrow 0$ .

Leveraging Eq. (10) and assuming  $\Delta t L < 1$ , Eq. (7) becomes

$$\|e_{n+1}\| \leq \frac{1 + 4\Delta t CL}{1 - \Delta t L} \|e_n\| + \frac{\Delta t}{1 - \Delta t L} \tau(\Delta t).$$

Let us define  $\alpha := 1 - \Delta t L$  and  $\beta := 1 + 4\Delta t CL$ . By recursion, we obtain:

$$\|e_{n+1}\| \leq \alpha^{-1} \Delta t \tau(\Delta t) \sum_{j=0}^n \beta^j \alpha^{-j} + (\beta \alpha^{-1})^{n+1} \|e_0\|,$$

where  $\|\mathbf{e}_0\| \equiv 0$ , so the last term cancels out. To treat the sum, we first bound  $\beta^j \leq \beta^{N_t}$ ,  $\forall j$ , and use the geometric sum for the remaining term in  $\alpha^{-j}$ :

$$\|\mathbf{e}_{n+1}\| \leq \alpha^{-1} \beta^{N_t} \Delta t \tau(\Delta t) \frac{\alpha^{-(n+1)} - 1}{\alpha^{-1} - 1} = (\beta^{N_t} \Delta t \tau(\Delta t)) \alpha^{-1} \frac{\alpha^{-(n+1)} - 1}{\alpha^{-1} - 1}.$$

The terms in  $\alpha$  develop as follows:

$$\alpha^{-1} \frac{\alpha^{-(n+1)} - 1}{\alpha^{-1} - 1} = \alpha^{-1} \frac{\alpha^{-(n+1)} - 1}{\frac{\Delta t L}{\alpha}} = \frac{\alpha^{-(n+1)} - 1}{\Delta t L} \leq \frac{e^{\Delta t(n+1)L} - 1}{\Delta t L}$$

where we exploited the fact that  $(1 - x) < e^{-x}$ . On the whole,

$$\|\mathbf{e}_{n+1}\| \leq \beta^{N_t} \frac{e^{TL} - 1}{L} \tau(\Delta t).$$

Finally, since  $\beta^{N_t} = (1 + 4C\Delta t L)^{N_t} \leq e^{4CTL}$ , we have:

$$\|\mathbf{e}_{n+1}\| \leq \frac{e^{TL} - 1}{L} e^{4CTL} \tau(\Delta t).$$

Therefore, the error is bounded by the product of the constant  $\frac{e^{TL}-1}{L}$  times an  $\mathcal{O}(\Delta t)$  term ( $e^{4CTL} \tau(\Delta t)$ ), which completes the proof.  $\square$

**Remark 2.4.** In the proof, we assumed that  $\|\mathbf{y}(t_n)\|$  does not vanish. When  $\|\mathbf{y}(t_n)\|$  falls below  $K_1 \Delta t$  ( $K_1 \in \mathbb{R}^+$ ), we set  $\tilde{\mathbf{V}}_n = [1, 0, \dots, 0]^T$ . Then  $\|\tilde{\mathbf{V}}_n - \mathbf{V}_n\| \leq 2$ , and by continuity of the analytical solution, we have  $\|\mathbf{y}(t_{n+1})\| \leq K_2 \Delta t$  as well. Therefore, Eq. (9) rewrites as

$$\left\| \tilde{\mathbf{V}}_n \tilde{\mathbf{V}}_n^T \mathbf{y}(t_{n+1}) - \mathbf{V}_n \mathbf{V}_n^T \mathbf{u}_{n+1} \right\| \leq 4 \|\mathbf{y}(t_{n+1})\| + \|\mathbf{e}_{n+1}\| \leq 4K_2 \Delta t + \|\mathbf{e}_{n+1}\|,$$

which yields

$$\|\mathbf{e}_{n+1}\| \leq \|\mathbf{e}_n\| + \Delta t L \|\mathbf{e}_{n+1}\| + 2K_2 L \Delta t^2 + \Delta t \tau(\Delta t).$$

Now, the  $\mathcal{O}(\Delta t^2)$  term can be combined with the global truncation error to complete the proof as above.

**Corollary 2.5.** The IMEX–RB scheme is zero–stable.

*Proof.* By the Lax–Richtmyer equivalence theorem [33, p. 41], a consistent and convergent method is zero–stable.  $\square$

## 2.4 Absolute stability of IMEX–RB

We study the absolute stability of IMEX–RB when applied to the model problem:

$$\begin{cases} \mathbf{y}'(t) = \mathbf{A}\mathbf{y}(t) & t \in I, \\ \mathbf{y}(0) = \mathbf{y}_0, \end{cases}$$

where  $\mathbf{A} \in \mathbb{R}^{N_h \times N_h}$  is supposed to be a diagonalizable matrix with eigenvalues  $\{\lambda_i\}_{i=1}^{N_h} \in \mathbb{C}$  satisfying  $\text{Re}\{\lambda_i\} < 0$ ,  $i = 1, \dots, N_h$ . By definition of absolute stability, we aim to prove:

$$\lim_{n \rightarrow +\infty} \|\mathbf{u}_{n+1}\| = 0.$$

**Theorem 2.6** (Absolute stability of IMEX–RB). Let  $\mathbf{A} = \mathbf{T}\mathbf{\Lambda}\mathbf{T}^{-1} \in \mathbb{R}^{N_h \times N_h}$  be a diagonalizable matrix, with  $N_h$  distinct eigenvalues having negative real parts and ordered as  $|\lambda_{N_h}| > |\lambda_{N_h-1}| > \dots > |\lambda_1| > 0$ . Let  $\mu := \min_i |\text{Re}\{\lambda_i\}|$ . Suppose that at each timestep  $t_n$  the reduced basis matrix  $\mathbf{V}_n \in \mathbb{R}^{N_h \times N}$  satisfies:

$$\|(\mathbf{I} - \mathbf{V}_n \mathbf{V}_n^T) \mathbf{u}_{n+1}\| \leq \varepsilon \|\mathbf{u}_{n+1}\|, \quad (11)$$

where  $\varepsilon$  is such that

$$0 \leq \varepsilon < \frac{\mu}{|\lambda_{N_h}| K_2(\mathbf{T})} \leq 1. \quad (12)$$

Here,  $K_2(\mathbf{T}) = \|\mathbf{T}\| \|\mathbf{T}^{-1}\|$  is the condition number of the eigenvectors matrix  $\mathbf{T}$  in the spectral norm. Then the IMEX–RB scheme is absolutely stable.

*Proof.* We switch to modal coordinates by defining  $\mathbf{v}_{n+1} := \mathbf{T}^{-1} \mathbf{u}_{n+1}$ . Left-multiplying the IMEX–RB scheme of Eq. (4) by  $\mathbf{T}^{-1}$  yields:

$$\mathbf{v}_{n+1} = \mathbf{v}_n + \Delta t \mathbf{\Lambda} \mathbf{T}^{-1} \mathbf{V}_n \mathbf{V}_n^T \mathbf{u}_{n+1}.$$

This expression can be rewritten as:

$$\mathbf{v}_{n+1} = \mathbf{v}_n + \Delta t \mathbf{\Lambda} \mathbf{v}_{n+1} - \Delta t \mathbf{\Lambda} \mathbf{T}^{-1} (\mathbf{I} - \mathbf{V}_n \mathbf{V}_n^T) \mathbf{u}_{n+1},$$

and thus

$$\mathbf{v}_{n+1} = (\mathbf{I} - \Delta t \mathbf{\Lambda})^{-1} [\mathbf{v}_n - \Delta t \mathbf{\Lambda} \mathbf{T}^{-1} (\mathbf{I} - \mathbf{V}_n \mathbf{V}_n^T) \mathbf{u}_{n+1}]. \quad (13)$$

Let  $\mu = \min_i |\operatorname{Re}\{\lambda_i\}| > 0$ . Since for any  $z \in \mathbb{C}$ , it holds  $|\frac{1}{z}| = \frac{1}{|z|} \leq \frac{1}{|\operatorname{Re}\{z\}|}$ , we have

$$\|(\mathbf{I} - \Delta t \mathbf{\Lambda})^{-1}\| = \max_i \left| \frac{1}{1 - \Delta t \lambda_i} \right| \leq \frac{1}{1 + \Delta t \mu}.$$

Taking the norm of Eq. (13), exploiting the assumption in Eq. (11) and that  $\|\mathbf{u}_{n+1}\| \leq \|\mathbf{T}\| \|\mathbf{v}_{n+1}\|$ , we obtain:

$$\|\mathbf{v}_{n+1}\| \leq \frac{1}{1 + \Delta t \mu} \left[ \|\mathbf{v}_n\| + \Delta t \varepsilon |\lambda_{N_h}| K_2(\mathbf{T}) \|\mathbf{v}_{n+1}\| \right],$$

where we used  $\|\mathbf{\Lambda}\| = |\lambda_{N_h}|$ . Rearranging terms gives:

$$\left( 1 - \frac{\Delta t \varepsilon |\lambda_{N_h}| K_2(\mathbf{T})}{1 + \Delta t \mu} \right) \|\mathbf{v}_{n+1}\| \leq \frac{1}{1 + \Delta t \mu} \|\mathbf{v}_n\|.$$

Under the condition  $\varepsilon < \frac{1 + \Delta t \mu}{\Delta t |\lambda_{N_h}| K_2(\mathbf{T})} =: C_1$ , the multiplicative factor in the left-hand side is positive and the bound is nontrivial. Therefore, the scheme is absolutely stable provided that:

$$\frac{1}{1 + \Delta t \mu - \Delta t \varepsilon |\lambda_{N_h}| K_2(\mathbf{T})} < 1 \quad \iff \quad \varepsilon < \frac{\mu}{|\lambda_{N_h}| K_2(\mathbf{T})} =: C_2. \quad (14)$$

Since  $C_2 < C_1$ ,  $C_2$  constitutes the most restrictive bounding term. Under the condition  $\varepsilon < C_2$ , we conclude that  $\|\mathbf{v}_{n+1}\| \rightarrow 0$  as  $n \rightarrow +\infty$ . Since  $\|\mathbf{u}_{n+1}\| \leq \|\mathbf{T}\| \|\mathbf{v}_{n+1}\|$ , it follows  $\lim_{n \rightarrow +\infty} \|\mathbf{u}_{n+1}\| = 0$ , which proves the absolute stability of the IMEX–RB scheme.  $\square$

The quantity  $\varepsilon$  introduced in Eq. (11) is a stability tolerance. By analogy with the canonical RB method, it corresponds to the proper orthogonal decomposition error tolerance on  $\mathbf{u}_{n+1}$ . If  $\mathbf{A}$  is symmetric, then  $\mu = |\lambda_1|$ ,  $K_2(\mathbf{T}) = 1$ ; hence, Eq. (12) simplifies to  $\varepsilon \leq K_2(\mathbf{A})^{-1} =: \bar{\varepsilon}$ . As a result, the worse the condition number of  $\mathbf{A}$ , the smaller the value of  $\varepsilon$  required to satisfy the inequality in Eq. (11). If  $\mathbf{A}$  is not symmetric, the theoretical bound  $C_2$  reported in Eq. (14) is always lower than  $\bar{\varepsilon}$ . Since computing  $C_2$  is generally impractical, in our numerical tests we set  $\varepsilon = \gamma \bar{\varepsilon}$ ,  $\gamma \in \mathbb{R}^+$ , to derive a computationally affordable educated guess.

## 2.5 The IMEX–RB algorithm

In Algorithm 1, we describe the IMEX–RB algorithm and its computational costs in detail.

At time  $t_n$ , we perform the steps of Eqs. (2)–(3), to compute  $\mathbf{u}_{n+1}$ . This requires assembling a basis  $\mathbf{V}_n$  satisfying the inequality of Eq. (11) for a given value of  $\varepsilon$  subject to the condition of Eq. (12). Aiming to meet the stability condition, and motivated by the intuition that past solutions can be exploited to compute an accurate extrapolation of the new solution  $\mathbf{u}_{n+1}$ , we define the  $\mathbf{V}_n$  as an orthonormal basis for the subspace  $\mathcal{V}_n = \operatorname{span}\{\mathbf{u}_{n-N_n+1}, \dots, \mathbf{u}_n\}$ , for some  $N_n := \min\{N, n\} \in \mathbb{N}^+$  (line 4). The user–defined value of  $N$  is problem–dependent: it should be increased for larger values of  $N_h$  or larger values of  $\Delta t$ . As a rule of thumb, in the numerical tests we always select  $N$  to be on the order of tens, even for problems with up to  $10^5$  degrees of freedom.

However, choosing the so–defined reduced basis size may not be sufficient to satisfy the inequality of Eq. (11) for a given  $\varepsilon \in \mathbb{R}^+$ . Therefore, we introduce a loop (line 6), thus allowing for “inner” iterations, solving Eqs. (2)–(3) for  $k = 0, 1, \dots$  (lines 7–8) and generating a sequence of iterates  $\mathbf{u}_{n+1}^{(k)}$ . Such iterates are used to conveniently enrich the reduced subspace, until Eq. (11) holds. To do so, we define an initial orthonormal basis  $\mathbf{V}_n^{(0)}$  so that  $\mathcal{V}_n^{(0)} = \operatorname{span}\{\mathbf{u}_{n-N_n+1}, \dots, \mathbf{u}_n\}$  and assemble the basis by means of a QR decomposition. Then, after each inner iteration, if the absolute stability criterion is not met (line 10), we augment the reduced basis with the orthogonal complement of the current iterate  $\mathbf{u}_{n+1}^{(k)}$ , performing one step of the Gram–Schmidt orthogonalization procedure (line

**Algorithm 1** IMEX–RB algorithm

**Require:**  $\mathbf{y}_0$ : initial condition;  $N_t$ : number of timesteps,  $\varepsilon$ : absolute stability parameter;  $N$ : default reduced subspace dimension;  $M$ : maximal number of inner iterations.

```

1:  $n \leftarrow 0$ 
2:  $\mathbf{u}_0 \leftarrow \mathbf{y}_0$ 
3: while  $n < N_t$  do
4:    $\mathbf{V}_n^{(0)}, \mathbf{R}_n \leftarrow \text{QR}(\mathbf{u}_{n-N_n+1}, \dots, \mathbf{u}_n)$  ▷ Basis assembly –  $\mathcal{O}(N_h N_n)$ 
5:    $k \leftarrow 0$ 
6:   while  $k < M$  do
7:     Solve  $\delta \mathbf{u}_{n+1}^N - \Delta t \mathbf{V}_n^{(k)T} \mathbf{f}(t_{n+1}, \mathbf{V}_n^{(k)} \delta \mathbf{u}_{n+1}^N + \mathbf{u}_n) = \mathbf{0}$  ▷ RB step –  $\mathcal{O}(L(N_h^2 + N_h N_k + N_k^3))$ 
8:      $\mathbf{u}_{n+1}^{(k)} \leftarrow \mathbf{u}_n + \Delta t \mathbf{f}(t_{n+1}, \mathbf{V}_n^{(k)} \delta \mathbf{u}_{n+1}^N + \mathbf{u}_n)$  ▷ Explicit FOM step –  $\mathcal{O}(N_h^2)$ 
9:      $\mathbf{r}_{n+1}^{(k)} \leftarrow (\mathbf{I} - \mathbf{V}_n^{(k)} \mathbf{V}_n^{(k)T}) \mathbf{u}_{n+1}^{(k)}$ 
10:    if  $\|\mathbf{r}_{n+1}^{(k)}\| / \|\mathbf{u}_{n+1}^{(k)}\| < \varepsilon$  then ▷ Stability condition –  $\mathcal{O}(N_h N_k)$ 
11:      break
12:    end if
13:     $\mathbf{V}_n^{(k+1)} \leftarrow [\mathbf{V}_n^{(k)} \mid \mathbf{r}_{n+1}^{(k)} / \|\mathbf{r}_{n+1}^{(k)}\|]$  ▷ Basis enrichment –  $\mathcal{O}(N_h N_k)$ 
14:     $k \leftarrow k + 1$ 
15:  end while
16:   $\mathbf{u}_{n+1} \leftarrow \mathbf{u}_{n+1}^{(k)}$ 
17:   $\mathbf{V}_n \leftarrow \mathbf{V}_n^{(0)}$ 
18:   $n \leftarrow n + 1$ 
19: end while

```

13). Hence, at the  $k$ –th inner iteration, the reduced basis matrix  $\mathbf{V}_n^{(k)}$  has  $N_k := N_n + k$  columns. A maximum number  $M \in \mathbb{N}$  of inner iterations is allowed, so that the maximal size the reduced basis can attain is  $\tilde{N} := N_n + M - 1$ . We highlight that  $M$  is a user–defined parameter, which should be set sufficiently large (e.g.,  $M = 100$ ). If the algorithm fails to satisfy the stability condition in Eq. (11) within  $M$  inner iterations, the procedure should be terminated, and larger values of  $M$  and/or  $N$  should be considered.

Once the absolute stability condition is satisfied, say after  $K \in \mathbb{N}$ ,  $K \leq M$ , inner iterations, we identify the approximate solution  $\mathbf{u}_{n+1}$  as the last available iterate  $\mathbf{u}_{n+1}^{(K)}$  (line 16). Therefore, with reference to the previous theoretical analysis, we identify the subspace  $\mathcal{V}_n := \mathcal{V}_n^{(K)}$ , spanned by the columns of  $\mathbf{V}_n := \mathbf{V}_n^{(K)}$ .

The QR decomposition in line 4 reduces to a QR update, which can be efficiently computed using well–established algorithms [34, 35]. Specifically, by updating the existing reduced basis matrix  $\mathbf{V}_{n-1} \in \mathbb{R}^{N_h \times N_{n-1}}$ , obtained via QR decomposition of the snapshot matrix  $[\mathbf{u}_{n-N_{n-1}+1}, \dots, \mathbf{u}_{n-1}]$  at timestep  $n-1$ , the QR factorization within IMEX–RB incurs a computational cost of  $\mathcal{O}(N_h N_n)$  and is performed once per timestep. At step  $n = 0$ , the basis is initialized as  $\mathbf{V}_0 \in \mathbb{R}^{N_h \times 1}$ , which consists solely of the normalized initial condition. If the initial condition is identically zero, we define the basis as the unit vector  $[1 \ 0 \ \dots \ 0]^T$ . Besides, if, at time  $t_n$ , the QR update fails because  $\mathbf{u}_n$  lies in the previous subspace spanned by  $\mathbf{V}_{n-1}$  up to a defined tolerance, the update is skipped.

Furthermore, numerical experiments suggest that it is better to discard the contribution of inner iterates in the basis to compute the solution at the subsequent timestep. This is justified by the observation that iterates are likely to introduce undesired numerical oscillations, jeopardizing the method’s performance. Therefore, at time  $t_{n+1}$ , the initial basis  $\mathbf{V}_{n+1}^{(0)}$  is computed with a QR update of  $\mathbf{V}_n^{(0)}$ , to span the subspace identified by the snapshot matrix  $[\mathbf{u}_{n-N_{n+1}+2}, \dots, \mathbf{u}_{n+1}]$ . Therefore, in line 17 in the IMEX–RB algorithm, we discard the enrichment of  $\mathbf{V}_n$  computed during the inner iterations.

**Remark 2.7.** *The proof of Theorem 2.3 assumes  $\mathcal{V}_n = \text{span}\{\mathbf{u}_n\}$  only. As explained above, the IMEX–RB algorithm enables the reduced basis  $\mathbf{V}_n$  to span a larger subspace than  $\text{span}\{\mathbf{u}_n\}$ , so that  $\mathcal{V}_n \supseteq \text{span}\{\mathbf{u}_n\}$ . This extra richness is what ensures the absolute stability of the IMEX–RB method. However, we remark that our convergence analysis is not affected by these extra directions of  $\mathbf{V}_n$  as  $\Delta t \rightarrow 0$ . In particular, by construction of the IMEX–RB algorithm,*

given a  $z \in \mathcal{V}_n$ , we have

$$\left\| \frac{\mathbf{u}_n \mathbf{u}_n^T}{\|\mathbf{u}_n\|^2} z - z \right\| \rightarrow 0 \quad \text{as } \Delta t \rightarrow 0,$$

i.e. the reduced subspace converges to  $\text{span}\{\mathbf{u}_n\}$  as the timestep size goes to zero. This may allow extending the proof of Theorem 2.3 to the case  $N > 1$ .

**Remark 2.8.** In the proof of absolute stability (Theorem 2.6), the term  $-\varepsilon|\lambda_{N_h}|K_2(T)$  in the denominator of Eq. (14) imposes an upper bound on the permissible value of  $\varepsilon$  to ensure stability at each time step. This estimate reflects a worst-case scenario in which the dynamics associated with the most numerically unstable eigenvalue  $\lambda_{N_h}$  are not treated implicitly. However, by construction, the IMEX–RB method enforces alignment of the reduced basis with the dominant modes of the solution at time  $\mathbf{u}_{n+1}$ . If the mode corresponding to  $\lambda_{N_h}$  is captured by the basis, it is automatically included in the implicit step. The actual stability threshold on  $\varepsilon$  may be less restrictive than the derived bound of Eq. (12). Numerical testing is mandatory to assess its required value.

## 2.6 Computational costs

We now perform a comprehensive analysis of the computational cost of the IMEX–RB algorithm.

Let  $J \in \mathbb{N}^+$  be the maximal number of iterations of the nonlinear solver, used to solve the reduced implicit step at each inner iteration. For simplicity, let us suppose that at each iteration the basis has the maximal size  $\tilde{N} = M + N - 1$ . The overall complexity of *one timestep* of IMEX–RB is obtained by summing up the costs of all steps of the algorithm:

- $\mathcal{O}(N_h^2)$  operations for assembling the full–order Jacobian at each timestep. We opt for a quasi–Newton method, to assemble the Jacobian only once per timestep;
- $\mathcal{O}(MJ(N_h^2 + N_h\tilde{N} + \tilde{N}^3))$  operations for the implicit RB step using the quasi–Newton method. This accounts for the evaluation/assemble of  $\mathbf{f}$  (generally involving matrix–vector products, thus  $\mathcal{O}(N_h^2)$ ), its projection onto the reduced subspace ( $\mathcal{O}(N_h\tilde{N})$ ) and the solution of a small dense linear system ( $\mathcal{O}(\tilde{N}^3)$ ) for up to  $L$  nonlinear solver iterations and up to  $M$  inner iterations;
- $\mathcal{O}(N_h^2M)$  operations for the explicit step, which only involves matrix–vector products to compute  $\mathbf{u}_{n+1}$ ;
- $\mathcal{O}(MN_h\tilde{N})$  operations for evaluating the stability criterion on  $\mathbf{u}_{n+1}$ ;
- $\mathcal{O}(MN_h\tilde{N})$  operations to enrich the reduced basis matrix through the Gram–Schmidt procedure.

Therefore, under the assumption that  $\tilde{N} \ll N_h$ , the repeated evaluation of the function  $\mathbf{f}$ , scaling as  $\mathcal{O}(N_h^2)$ , can be the bottleneck of the algorithm. Moreover, the adoption of a quasi–Newton approach to deal with nonlinearities and the Gram–Schmidt enrichment of the reduced basis entail that the assembly and enrichment of the reduced Jacobian only have a marginal dependency on  $M$ . Indeed, once the full–order Jacobian is assembled and projected onto the initial reduced subspace at the beginning of the timestep, which has a cost of  $\mathcal{O}(N_h^2N_n)$ , inner updates of the reduced Jacobian require only  $\mathcal{O}(N_h\tilde{N})$  operations per iteration. To produce a fair comparison of computational times, the same quasi–Newton approach is also employed with the backward Euler method. Nonetheless, the complexity of the latter scales as  $\mathcal{O}(N_h^3)$  per nonlinear iteration. Therefore, computational gains are expected.

Regarding memory storage, at each time step, thanks to the QR update procedure, it is sufficient to store only  $\mathbf{R}_n$  of size  $N_n \times N_n$ , without retaining the full matrix of physical snapshots. Additionally, the basis matrix  $\mathbf{V}_n$  must be stored, which is enriched during subiterations up to a maximum dimension  $N_h \times \tilde{N}$ .

**Remark 2.9.** In the above analysis, we did not account for the sparsity of the full–order Jacobian matrix, which is in fact of primary importance when estimating computational costs. Indeed, sparse linear systems arising from suitable spatial discretizations of PDEs can often be solved in  $\mathcal{O}(N_h^2)$  operations instead of  $\mathcal{O}(N_h^3)$ , using preconditioned iterative methods such as GMRES [35]. Similarly, favorable sparsity patterns allow full–order matrix–vector products to be performed in less than  $\mathcal{O}(N_h^2)$  operations. As a result, the actual computational gains of IMEX–RB over backward Euler are highly problem–dependent and cannot be predicted a priori. Therefore, they should be investigated numerically.

### 3 Numerical results

In this section, we present the numerical experiments we conducted to assess the behavior of the IMEX–RB method and we discuss the obtained results.

In all numerical tests, we consider a spatial computational domain of the form  $\Omega = [0, L]^d \subset \mathbb{R}^d$  ( $d = 2, 3$ ). The problem is discretized in space by finite differences on a uniform Cartesian grid, made of  $N_i$  nodes for each dimension  $i = 1, \dots, d$ . This entails a total of  $N_h = K \prod_{i=1}^d N_i$  DOFs,  $K$  being the number of solution components. Also, we denote by  $h_i := L/(N_i - 1)$  the grid spacing in each dimension. In the following, we set  $h_i = h$ , i.e. we employ the same discretization along all dimensions. The time interval  $[0, T]$  is instead partitioned into  $N_t$  uniform sub–intervals of size  $\Delta t := T/N_t$ .

The performances of IMEX–RB are expressed in terms of its errors and computational times, and are compared against those of the backward Euler (BE) method, which serves as a baseline. Regarding the error computation, we always assume the existence of an exact analytical solution  $\mathbf{u}_{\text{ex}} : \Omega \times [0, T] \rightarrow \mathbb{R}^K$ , which is evaluated at the grid points and whose components we denote by  $(\mathbf{u}_{\text{ex}})_k$ ,  $k = 1, \dots, K$ . Let  $\mathcal{I} = \{1, \dots, N_1\} \times \dots \times \{1, \dots, N_d\}$  denote the set of grid–point indices, so that  $\mathbf{i} = (i_1, \dots, i_d) \in \mathcal{I}$ ; let  $\mathbf{x}_{\mathbf{i}} = (x_{1,i_1}, \dots, x_{d,i_d})$  be the grid point associated with the multi–index  $\mathbf{i}$ . We define  $(\mathbf{u}_n)_{\mathbf{i},k}$  as the approximation of  $(\mathbf{u}_{\text{ex}}(\mathbf{x}_{\mathbf{i}}, t_n))_k$  yielded by the numerical method of choice. Then, the 2–norm relative error in space on the  $k$ –th solution component at time  $t_n$  is given by [36, p. 252]

$$e_{r,k}(t_n) := \frac{\left( \sum_{\mathbf{i} \in \mathcal{I}} h^d |(\mathbf{u}_n)_{\mathbf{i},k} - (\mathbf{u}_{\text{ex}}(\mathbf{x}_{\mathbf{i}}, t_n))_k|^2 \right)^{1/2}}{\left( \sum_{\mathbf{i} \in \mathcal{I}} h^d |(\mathbf{u}_{\text{ex}}(\mathbf{x}_{\mathbf{i}}, t_n))_k|^2 \right)^{1/2}} = \frac{\|\mathbf{e}_k(t_n)\|_2}{\|(\mathbf{u}_{\text{ex}}(\cdot, t_n))_k\|_2}, \quad k = 1, \dots, K. \quad (15)$$

Ultimately, the accuracies of IMEX–RB and BE are quantified by the following component–wise aggregate error indicator, which takes into account the behavior of the method over the entire time interval:

$$\bar{e}_{r,k} := \left( \frac{\sum_{n=1}^{N_t} \Delta t \|\mathbf{e}_k(t_n)\|_2^2}{\sum_{n=1}^{N_t} \Delta t \|(\mathbf{u}_{\text{ex}}(\cdot, t_n))_k\|_2^2} \right)^{1/2}, \quad k = 1, \dots, K. \quad (16)$$

For  $K = 1$ , we denote  $\bar{e}_{r,k}$  as  $\bar{e}_r$  for simplicity. Also, to empirically assess stability, we introduce the following metric:

$$\mathcal{E}_e(t_n) := \sum_{k=1}^K \|\mathbf{e}_k(t_n)\|_2^2. \quad (17)$$

Advective terms are approximated using second–order centered finite differences, while diffusive terms leverage second–order five–point stencil formulations. For the Burgers’ equation (see Section 3.2), the convective term is also treated with second–order centered finite differences. Inhomogeneous Dirichlet boundary conditions are strongly enforced, leveraging lifting techniques. In particular, the numerical solution is expressed as the sum of an unknown component, which evaluates to zero at the Dirichlet boundaries, and a known lifting component, defined to match the Dirichlet data. Notably, this strategy enables looking for solutions that belong to a vector space and inherently configures the low–dimensional space  $\mathcal{V}_n$  of IMEX–RB as a vector space itself.

The large and sparse linear systems, arising from the application of BE at each discrete timestep, are solved with the GMRES method [37], preconditioned through incomplete LU factorization, with a drop tolerance of  $5 \cdot 10^{-3}$ . The small dense linear systems associated with the use of IMEX–RB are instead handled using the direct solver implemented in the `SciPy` library.

All numerical simulations are performed on the *Jed* cluster of the *Scientific IT and Application Support (SCITAS)*<sup>2</sup> at EPFL. All runs are executed sequentially. To ensure sufficient memory per job, we request 10 CPUs for each 2D test and 20 CPUs for the 3D test.

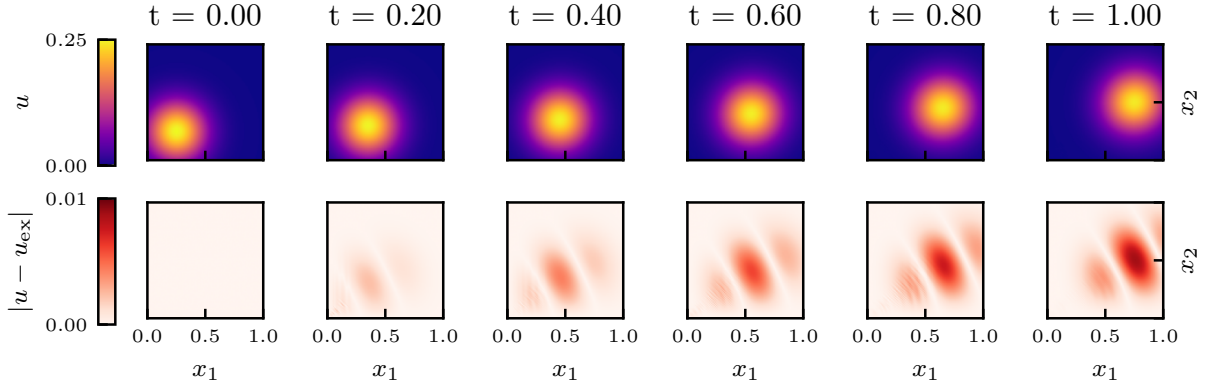


**Figure 1:** Numerical solution to Eq. (18), produced by IMEX–RB at five equispaced timesteps, and corresponding absolute error with respect to the exact solution. The results were obtained for  $N_1 = N_2 = 101$ ,  $N_t = 100$ ,  $\varepsilon = 2 \cdot 10^{-3}$ ,  $N = 10$  and  $M = 100$ .

### 3.1 Advection–diffusion equation in 2D

We consider the following two–dimensional linear advection–diffusion problem:

$$\begin{cases} \frac{\partial u}{\partial t} + c_x \frac{\partial u}{\partial x} + c_y \frac{\partial u}{\partial y} - \mu \Delta u = f, & \text{in } \Omega \times (0, T], \\ u = u_0, & \text{on } \Omega \times \{0\}, \\ u = g, & \text{on } \partial\Omega \times (0, T], \end{cases} \quad (18)$$

where  $\Omega = [0, 1]^2$ ,  $\partial\Omega \subset \mathbb{R}^2$  denotes its boundary, and  $T = 1$ . We consider a constant diffusion parameter  $\mu = 0.005$  and advection velocity  $\mathbf{c} = [c_x, c_y] = [0.5, 0.25]$ . The forcing term  $f : \Omega \times (0, T] \rightarrow \mathbb{R}$ , the initial condition  $u_0 : \Omega \rightarrow \mathbb{R}$ , and the Dirichlet datum  $g : \partial\Omega \times (0, T] \rightarrow \mathbb{R}$  are defined so that the exact solution to Eq. (18) writes as follows:

$$u_{\text{ex}}(\mathbf{x}, t) = U \exp\left(-\frac{\|\mathbf{x} - \mathbf{x}_0 - \mathbf{c}t\|_2^2}{\sigma^2 + \mu t}\right). \quad (19)$$

We note that  $\sigma > 0$  regulates the amplitude of the peak for the initial condition,  $U > 0$  is the peak solution value at  $t = 0$ , and  $\mathbf{x}_0 \in \Omega$  is the peak location at  $t = 0$ . In all the tests, we set  $\sigma = 0.25$ ,  $U = 0.25$ , and  $\mathbf{x}_0 = [0.25, 0.25]$ . From a qualitative standpoint, we remark that the solution consists of a traveling Gaussian blob, driven by the advection field, whose diffusion is fully counterbalanced by the external forcing term. Figure 1 reports the numerical solution obtained with IMEX–RB— for a specific spatio–temporal discretization of the domain and choice of the hyperparameters  $\varepsilon$ ,  $N$ ,  $M$  — at six equispaced timesteps, and the corresponding absolute errors with respect to the exact solution.

We start by empirically investigating the role of the stability tolerance  $\varepsilon$ . Figure 2a reports the relative errors — computed according to Eq. (16) — and the computational times, associated with BE and IMEX–RB for five different values of  $\varepsilon$ , seven different timestep sizes  $\Delta t_i = 2^{-i}$  for  $i = 4, \dots, 10$ , and two different mesh sizes  $h = 0.01$  and  $h = 0.005$  ( $N_i = 101, 201$ ). As reported in Section 2.4, the values of  $\varepsilon$  are chosen as multiples of  $\bar{\varepsilon} = (K_2(\mathbf{A}))^{-1}$ . Specifically, we have that  $\bar{\varepsilon} \approx 2.1 \cdot 10^{-3}$  for  $h = 0.01$  and  $\bar{\varepsilon} \approx 5.3 \cdot 10^{-4}$  for  $h = 0.005$ . We also report the timestep size  $\Delta t_{FE}$  below which the forward Euler method is stable. For the solution of the linear system in the BE steps, the GMRES tolerance is set to  $10^{-6}$ , as no noticeable differences in the solution error were observed when reducing it further. We begin by noting a few key observations. Firstly, if the timestep size  $\Delta t$  is sufficiently small, the errors of IMEX–RB are basically identical to those of BE and feature a linear convergence with respect to  $\Delta t$ . This result provides an empirical validation of Theorem 2.3. Secondly, if  $\varepsilon$  is sufficiently small (say,  $\varepsilon \lesssim 10 \bar{\varepsilon}$ ), IMEX–RB produces accurate results even for timestep values that lie well above the critical value for forward Euler. This result confirms that, upon suitable choices of the hyperparameters, the IMEX–RB scheme is stable, and also suggests that the bound of Eq. (12) might be too restrictive in practice. Additionally, we note that more stringent constraints on  $\varepsilon$  are required as  $h$  decreases, to obtain accurate solution approximations. In particular, we observe that, with both space discretizations, the errors of IMEX–RB diverge from those of BE as soon as  $\Delta t > \Delta t_{FE}$ , if  $\varepsilon$  is too large. This

<sup>2</sup><https://www.epfl.ch/research/facilities/scitas/hardware/>.

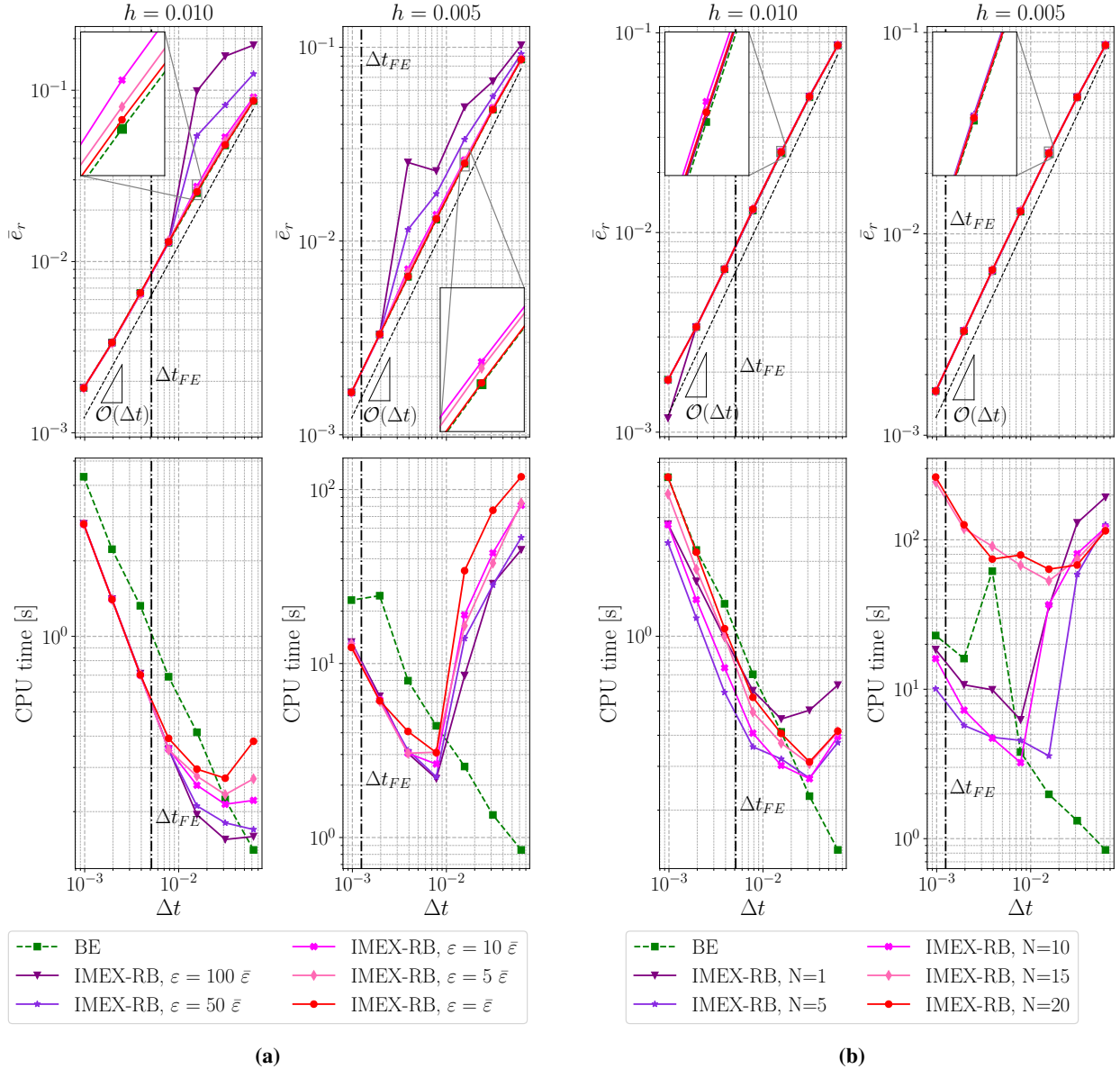


**Figure 2:** Backward Euler (BE) and IMEX–RB results on the 2D advection–diffusion problem: convergence analysis and CPU times (in seconds). (a) Results varying the stability tolerance  $\varepsilon$  (left:  $h = 0.01$ , right:  $h = 0.005$ ; IMEX–RB employs  $N = 10$ ,  $M = 100$ ). (b) Results varying the minimal reduced basis size  $N$  (left:  $h = 0.01$ , right:  $h = 0.005$ ; IMEX–RB employs  $\varepsilon = \bar{\varepsilon}$ ,  $M = 100$ ). CPU times are averaged over ten runs.

behavior could be easily inferred from the theory. Indeed, there exists an inverse proportionality relation between  $C_2$  — the stability tolerance upper bound in Eq. (10) — and the condition number of the system matrix, and the latter increases as the spatial grid gets refined.

Concerning computational efficiency, we observe that IMEX–RB outperforms BE for sufficiently small values of  $\Delta t$ , while BE is faster than IMEX–RB for large timestep values. In this regard, we underline that CPU runtimes of both algorithms strongly depend on the problem at hand, on the hardware specifics, and on the software implementation. As such, the reported times only offer indicative trends. Remarkably, the computational gains of IMEX–RB over BE are not limited to the case  $\Delta t < \Delta t_{FE}$ , where forward Euler is stable and hence configures as the first–order method of choice. Indeed, for both  $h = 0.01$  and  $h = 0.005$  and taking as reference the case  $\varepsilon = \bar{\varepsilon}$ , IMEX–RB is faster than BE until  $\Delta t \lesssim 5 \Delta t_{FE}$ . For instance, setting  $h = 0.005$  and  $\Delta t = 1/128 \approx 6 \Delta t_{FE}$ , the average runtimes of BE and IMEX–RB are, respectively 4.39 s and 3.07 s (–30%). The explosion of the computational times of IMEX–RB

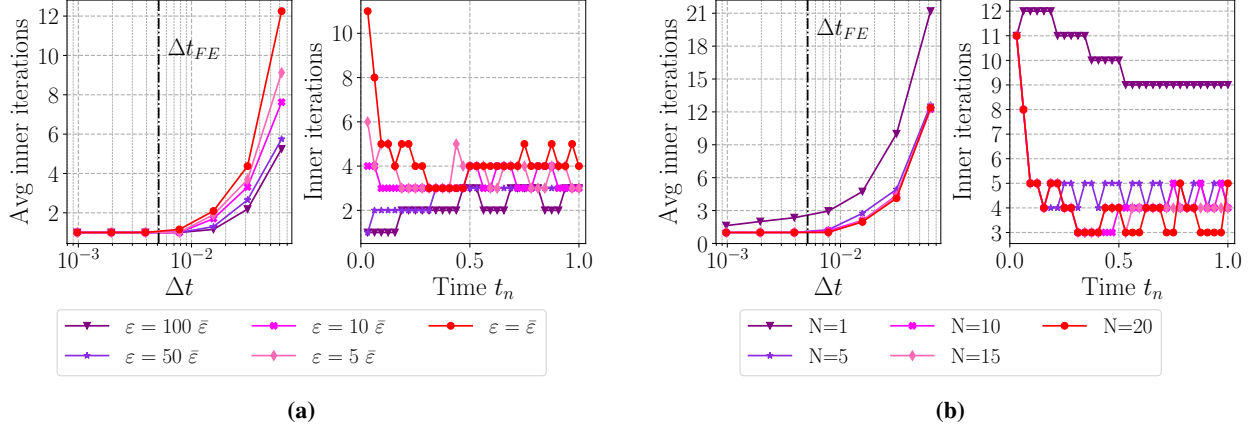


**Figure 3:** Number of inner iterations performed by the IMEX–RB method, on the 2D advection–diffusion problem. In particular, we investigate how the average number of inner iterations varies for different values of  $\Delta t$ , and the trend of iterations over time for  $\Delta t = 1/32$ . (a) Results varying the values of the stability tolerance  $\varepsilon$ ; (b) Results varying the reduced basis initial size  $N$ . All tests were conducted setting  $N_1 = N_2 = 101$  and a maximal number of inner iterations  $M = 100$ .

at large values of  $\Delta t$  can be justified by taking into account the number of inner iterations of the algorithm, which are shown in Figure 3a. As larger timestep values are employed, more iterations are required to satisfy the absolute stability constraint, which demands more computational resources. The number of inner iterations increases as smaller values of  $\varepsilon$  are selected. From Figure 3a, we note that the largest number of iterations occurs at the initial timesteps, where the solution history, and hence the baseline reduced basis dimension  $N$ , is small. As time progresses, only a few inner cycles (3 to 5 for  $\varepsilon = \bar{\varepsilon}$ ) are instead necessary to guarantee stability.

The performances of IMEX–RB considering different values of  $N$  are summarized in Figure 2b, where we report both relative errors and computational times, for timestep values  $\Delta t = 2^{-i}$ ,  $i = 4, \dots, 10$ , and mesh sizes  $h = 0.01$  and  $h = 0.005$ . For these numerical experiments, we set  $\varepsilon = \bar{\varepsilon}$ . Once again, we observe a linear decay of the error with respect to  $\Delta t$  and, for well–calibrated values of  $N$ , computational gains with respect to BE, if  $\Delta t \lesssim 5 \Delta t_{FE}$ . In particular, we remark that the discrepancy in performance for different values of  $N$  cannot be detected from the errors, but rather from the CPU runtimes. For  $N \geq 15$ , significantly higher computational times are observed for IMEX–RB, due to the repeated orthogonalizations required by the QR update procedure. This issue can be mitigated by relaxing the tolerance criterion used to skip the QR update. Furthermore, since the method allows for adaptive augmentation of the reduced basis via inner iterations, a small baseline value of  $N$  may lead to substantial growth of the low–dimensional subspace, thereby increasing the overall computational cost. Therefore, the performances can be optimized by choosing a value of  $N$  that is large enough to guarantee a good approximation of the solution manifold at each timestep, and small enough to save computational resources. Unfortunately, the optimal value of  $N$  is highly problem dependent, and *a priori* estimates are difficult to derive. For the test case at hand, as also demonstrated by the inner iterations results reported in Figure 3b, the best trade–off is offered by  $N = 5$ . For  $N = 1$ , many inner iterations are needed at all timesteps, which entails relevant costs for large timestep values; for  $N = 15$ , the reduced basis size is unnecessarily big, and IMEX–RB is never able to outperform BE.

### 3.2 Viscous Burgers’ equation in 2D

To assess the performance of IMEX–RB on a nonlinear PDE, we consider the following 2D viscous Burgers’ problem: find  $\mathbf{u} = [u_1, u_2]^T$  such that

$$\begin{cases} \frac{\partial \mathbf{u}}{\partial t} + (\mathbf{u} \cdot \nabla) \mathbf{u} - \nu \Delta \mathbf{u} = 0, & \text{in } \Omega \times (0, T], \\ \mathbf{u} = \mathbf{u}_0, & \text{on } \Omega \times \{0\}, \\ \mathbf{u} = \mathbf{g}, & \text{on } \partial\Omega \times (0, T], \end{cases} \quad (20)$$

where  $\Omega = [0, 1]^2$ ,  $\partial\Omega \subset \mathbb{R}^2$  denotes its boundary, and  $T = 1$ . The quantity  $\nu \in \mathbb{R}^+$  denotes the kinematic viscosity; in all tests, we set  $\nu = 10^{-2}$ . In particular, we consider a well–known benchmark problem [38, 39], whose analytical solution is given by

$$\mathbf{u}_{\text{ex}}(\mathbf{x}, t) = \frac{3}{4} - \frac{1}{4} \left[ \left( 1 + \exp \left( \frac{-4x_1 + 4x_2 - t}{1/32\nu} \right) \right)^{-1}, - \left( 1 + \exp \left( \frac{-4x_1 + 4x_2 - t}{1/32\nu} \right) \right)^{-1} \right]^T.$$

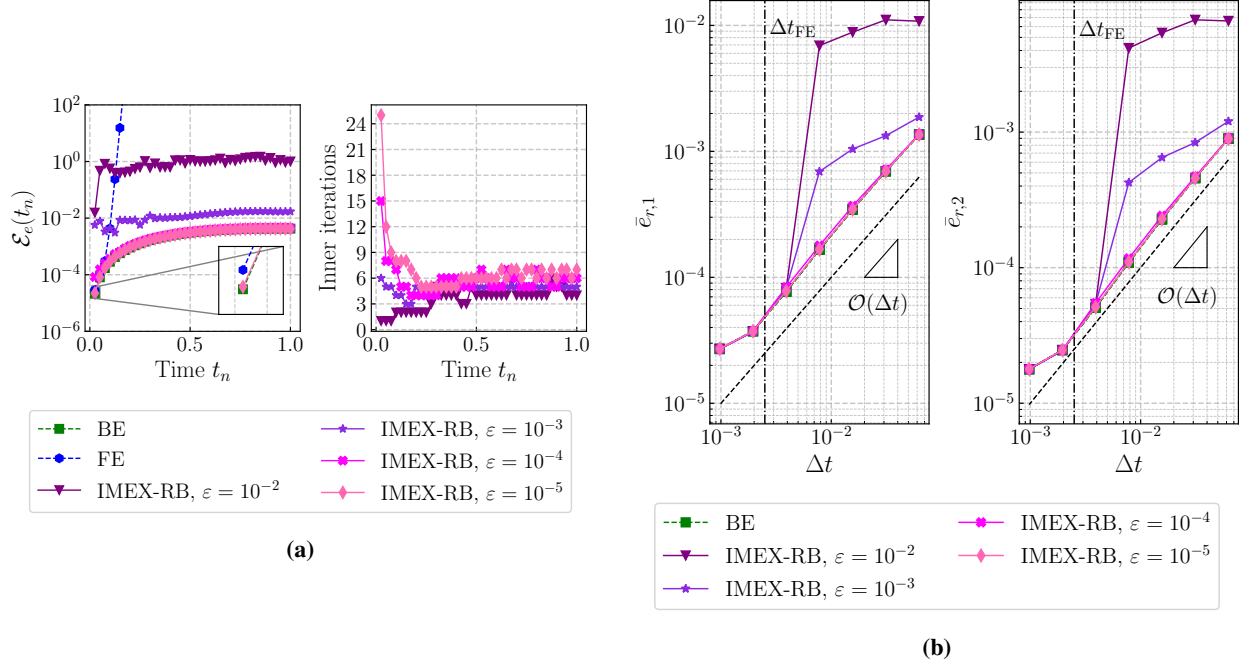


**Figure 4:** Backward Euler (BE) and IMEX–RB results on the 2D viscous Burgers’ equation. (a) Error metric  $\mathcal{E}(t_n)$  over time. In particular: (top) results for IMEX–RB, varying  $\varepsilon$ , BE and forward Euler (FE), setting  $N_t = 40$ ,  $N = 10$ ,  $M = 100$ . (bottom) number of inner iterations performed by IMEX–RB (bottom). (b) Convergence analysis of IMEX–RB on both solution components  $u_1$  (left) and  $u_2$  (right). FE is only stable for values of  $\Delta t$  to the left of the dashed line  $\Delta t_{FE}$ .

The initial condition  $\mathbf{u}_0 : \Omega \rightarrow \mathbb{R}^2$ , and the Dirichlet datum  $\mathbf{g} : \partial\Omega \times (0, T] \rightarrow \mathbb{R}^2$  are inferred from the exact solution.

At each time step, for both BE and IMEX–RB, a nonlinear system is solved using a quasi–Newton method. The Jacobian matrix of the PDE residual is assembled once at the beginning of the time step—evaluated at  $(t_{n+1}, \mathbf{u}_n)$ —and kept fixed throughout the iterations; in this context,  $\mathbf{u}_n$  acts as a first–order extrapolation of  $\mathbf{u}_{n+1}$ . The iterations are terminated when the Euclidean norm of the update falls below  $10^{-3} \cdot \Delta t$ , or at most after  $J = 100$  loops. The GMRES iterations used in the nonlinear solver are stopped once the relative residual — measured with respect to the norm of the right–hand side vector — is smaller than  $10^{-10}$ .

Unless differently specified, we set  $N_1 = N_2 = 101$  — for this choice, FE is stable for  $N_t \gtrsim 400$  — and a number of timesteps  $N_t = 40$ . For IMEX–RB, we consider a minimal reduced basis size  $N = 10$  and a maximal number of inner iterations  $M = 100$ . Since the nonlinear nature of the problem prevents computing a reliable estimate of the stability tolerance *a priori*, we empirically derive an educated guess by running *ad hoc* preliminary tests.

To showcase the absolute stability of IMEX–RB when varying  $\varepsilon$ , we investigate the trend of the metric  $\mathcal{E}_e$ , defined in Eq. (17). We fix both the space and time discretization, and we let  $\varepsilon = 10^{-i}$ ,  $i = 2, 3, 4, 5$ . Figure 4a shows both the trend of  $\mathcal{E}_e$  over time and the number of inner iterations performed by the IMEX–RB scheme. Firstly, we highlight that FE is numerically unstable for the selected value of  $N_t$ , since its error quickly explodes after a few timesteps. Secondly, if  $\varepsilon \geq 10^{-3}$ ,  $\mathcal{E}_e$  presents a jump with respect to that of BE already after the first timestep. This suggests that if the value of  $\varepsilon$  is too loose, some numerically unstable modes are immediately amplified by the explicit step, thus deteriorating accuracy. However, for the subsequent timesteps, setting  $\varepsilon = 10^{-2}$  suffices to keep the error bounded over the entire time interval, and the error discrepancy compared to BE is only due to what occurs at the initial timesteps. These considerations are also reflected in the observed number of inner iterations, which is significantly affected by the choice of  $\varepsilon$  only up to  $t_n \approx 0.2$ . For the following timesteps, all choices of  $\varepsilon$  lead to almost the same number of iterations, which indicates that the subspace quickly captures all the unstable modes necessary to meet the inequality of Eq. (11). Finally, this test case is exploited to define a value of  $\varepsilon$  to be used in the following experiments. Based on Figure 4a and aiming at an accuracy comparable to that of BE, we conclude that  $\varepsilon = 10^{-4}$  suffices to guarantee stability, without compromising accuracy.

As second numerical test, we perform a convergence study, keeping the spatial grid fixed ( $h = 0.01$ ) and varying the timestep sizes as  $\Delta t = 2^{-i}$  for  $i = 4, \dots, 10$ . Also, we change  $\varepsilon = 10^{-i}$ ,  $i = 2, \dots, 5$  to inspect how the stability tolerance affects convergence. As before, we fix  $N = 10$  and  $M = 100$ . At each timestep, the resulting

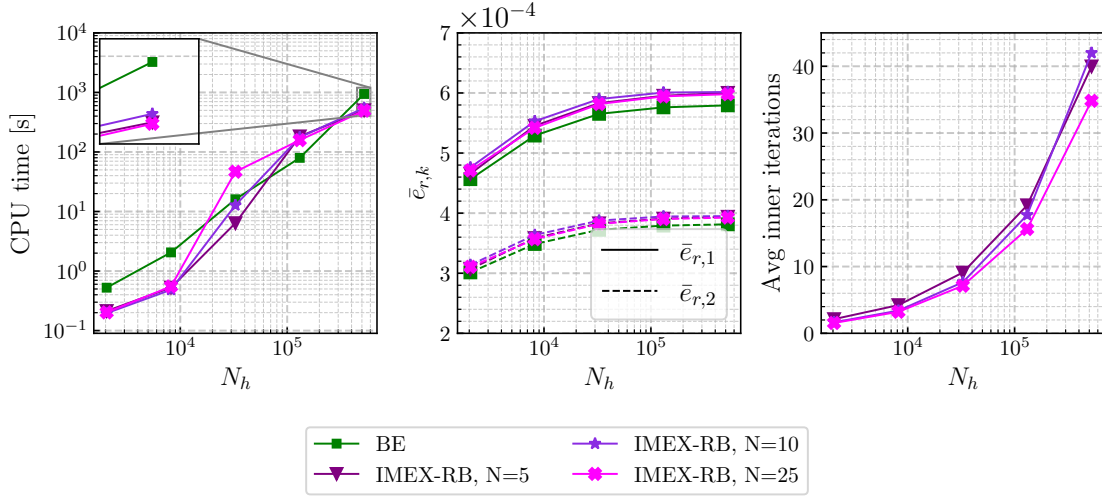


**Figure 5:** Backward Euler (BE) and IMEX–RB performances for different spatial discretizations, on the 2D viscous Burgers’ equation. In particular, we show CPU times (*left*) and errors (*center*) for BE and IMEX–RB, considering different values of  $N$ . Here, we set  $N_t = 40$  and  $\varepsilon = 10^{-4}$ . We also report the average number of inner iterations performed by IMEX–RB (*right*).

nonlinear system features approximately  $2 \cdot 10^4$  DOFs. For each choice of  $\Delta t$ , we compute the error according to the norm defined in Eq. (16). The results are displayed in Figure 4b, for both velocity components. In agreement with Theorem 2.3, IMEX–RB is convergent of order 1 in time. It can be noted that already for  $\varepsilon = 10^{-4}$ , the stability of IMEX–RB is reflected in the achieved accuracy, and for values of  $\Delta t$  above  $\Delta t_{FE}$ . On the contrary, for larger values of  $\varepsilon$ , despite meeting the bound of Eq. (11), absolute stability is not guaranteed, due to the premature termination of inner iterations.

Finally, in Figure 5, we compare the CPU times of BE and IMEX–RB, considering different spatial resolutions. Specifically, we set  $N_1 = N_2 = 2^i$  for  $i = 5, 6, \dots, 9$ , which results in up to  $N_h = 2N_1N_2 \approx 5 \times 10^5$  DOFs. We fix  $N_t = 40$ ,  $M = 100$ , and  $\varepsilon = 10^{-4}$ ; also, simulations are performed for  $N = 5, 10, 25$ . For each problem size, CPU times are averaged over five runs. In addition to CPU times, we report the error as defined in Eq. (16) and the average number of inner iterations performed by IMEX–RB. The CPU times of IMEX–RB are lower than those of BE for the smallest values of  $N_h$ , exhibit some variability with  $N$  as  $N_h$  increases, and fall, again below those of BE for the largest value of  $N_h$ . This behavior aligns with our expectations, since for large-scale problems, IMEX–RB is anticipated to be more computationally efficient than BE. At the same time, both schemes achieve comparable accuracy for all values of  $N_h$ , even for  $N = 5$ . As expected, the average number of inner iterations grows with  $N_h$ , since a larger full-order problem requires a higher-dimensional reduced subspace to capture the unstable modes. Nonetheless, the number of required iterations remains sufficiently low to yield computational advantages over BE.

Overall, the IMEX–RB scheme showcases superior computational efficiency compared to BE when applied to the problem in Eq. (20), while achieving comparable accuracy levels. Additionally, although increasing the reduced basis size  $N$  generally reduces the average number of inner iterations — especially for refined spatial grids — we observe that setting  $N = 5$  already yields satisfactory results in the considered scenario.

### 3.3 Advection–diffusion equation in 3D

We test IMEX–RB on the 3D counterpart of the problem of Eq. (18). The selected exact solution in this scenario is again given by Eq. (19), where this time  $\mathbf{x} = [x_1, x_2, x_3]^T$ . The exact solution satisfies the advection–diffusion equation with the following forcing term  $f: \Omega \times [0, T] \rightarrow \mathbb{R}$ :

$$f(\mathbf{x}, t) = U \frac{\mu \|\mathbf{x} - \mathbf{x}_0 - \mathbf{c}t\|_2^2 + 2\mu(3\mu t + 3\sigma^2 - 2\|\mathbf{x} - \mathbf{x}_0 - \mathbf{c}t\|_2^2)}{(\sigma^2 + \mu t)^2} \exp\left(-\frac{\|\mathbf{x} - \mathbf{x}_0 - \mathbf{c}t\|_2^2}{\sigma^2 + \mu t}\right).$$

We solve in the domain  $\Omega = [0, 1]^3$ , employing two different discretizations  $N_i = 51$  and  $N_i = 81$ ,  $i = 1, 2, 3$ . Furthermore, we select  $\mathbf{c} = [0.5, 0.25, 0.25]^T$  and  $\mathbf{x}_0 = [0.25, 0.25, 0.25]^T$ ,  $\sigma = 0.25$ ,  $\mu = 10^{-2}$ . For this test case, we are interested in studying how the IMEX–RB scheme behaves when increasing the dimension of the physical problem and the number of DOFs.

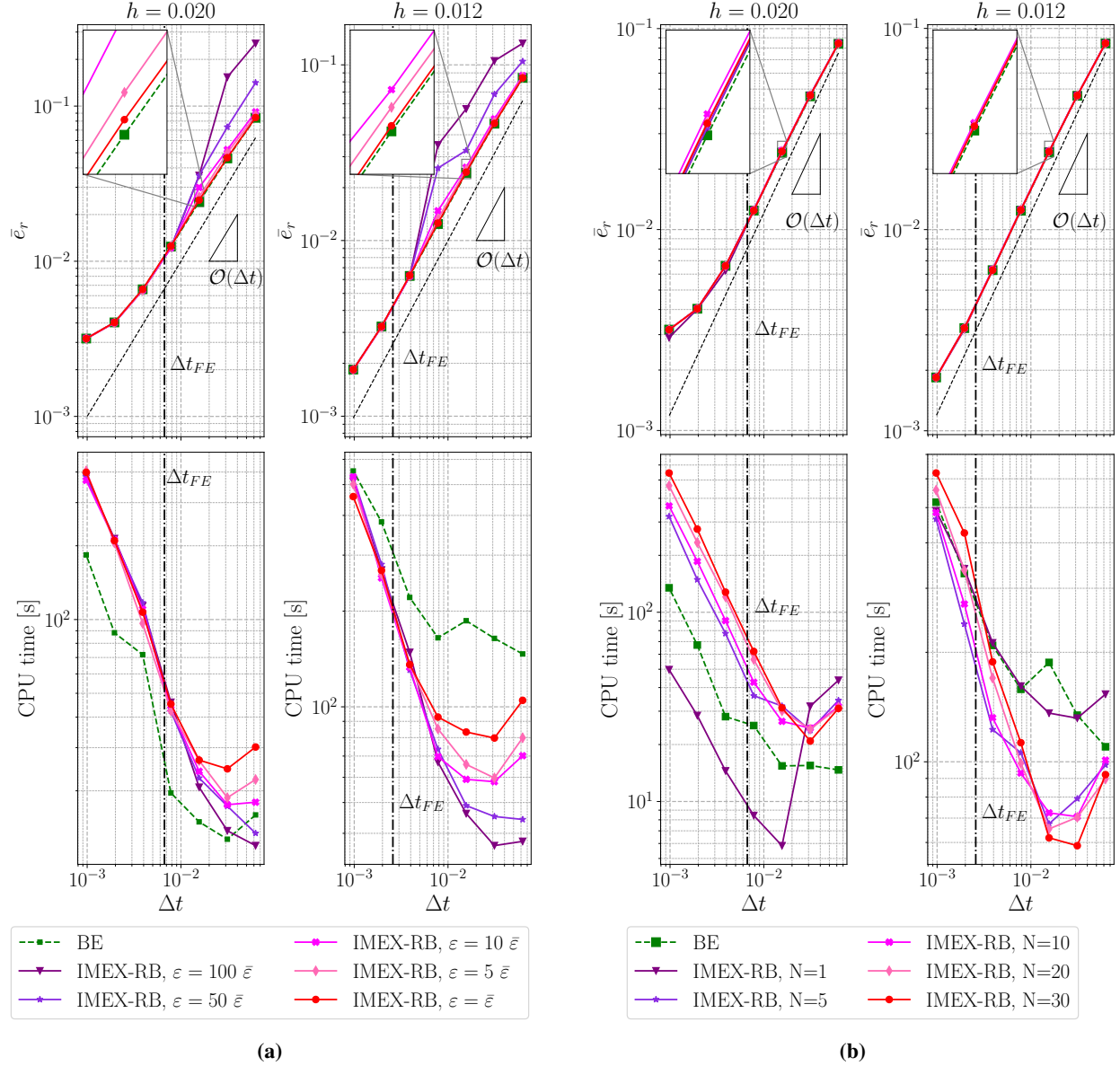


**Figure 6:** Comparison of backward Euler (BE) and IMEX–RB on the 3D advection–diffusion problem: study of convergence and CPU times in seconds. (a) Varying the hyperparameter  $\varepsilon$  (left:  $h = 0.02$ , right:  $h = 0.012$ ; IMEX–RB employs  $N = 10$ ,  $M = 100$ ). (b) Varying the minimal reduced basis size  $N$  (left:  $h = 0.02$ , right:  $h = 0.012$ ; IMEX–RB employs  $\varepsilon = \bar{\varepsilon}$ ,  $M = 100$ ). To save computational resources, the CPU times in this scenario are not averaged.

We begin by studying its convergence and the corresponding CPU times, for two different mesh sizes,  $h = 0.02$  and  $h = 0.012$ , and varying the value of  $\varepsilon$  with respect to  $\bar{\varepsilon} = K_2(\mathbf{A})^{-1}$ . In particular, we vary  $\Delta t = 2^{-i}$ ,  $i = 4, \dots, 10$ ; we obtain  $\bar{\varepsilon} \approx 3.28 \cdot 10^{-3}$  and  $\bar{\varepsilon} \approx 1.31 \cdot 10^{-3}$  for the considered mesh sizes<sup>3</sup>. Figure 6a displays the results. With respect to the same test conducted on the 2D problem (see Figure 2), we remark a similar behavior in convergence, for both values of  $h$  considered:  $\varepsilon \lesssim 10 \bar{\varepsilon}$  suffices to attain an error comparable to that of BE. Besides, the two–step approach of IMEX–RB makes it possible to achieve numerical stability for values of  $\Delta t$  well above the critical value for forward Euler  $\Delta t_{FE}$ . Moreover, Theorem 2.3 is once more validated, as we observe that the error behaves as  $\mathcal{O}(\Delta t)$ . Regarding CPU times, while keeping in mind the limits of the measured times, we highlight that for  $h = 0.02$ , IMEX–RB is less efficient than BE. As the problem grows in size, the  $\mathcal{O}(N_h^3)$  cost paid by BE makes IMEX–RB more

<sup>3</sup>To speed up the computations, the condition number of  $\mathbf{A}$  is obtained as ratio of singular values computed up to a tolerance of  $10^{-2}$ .

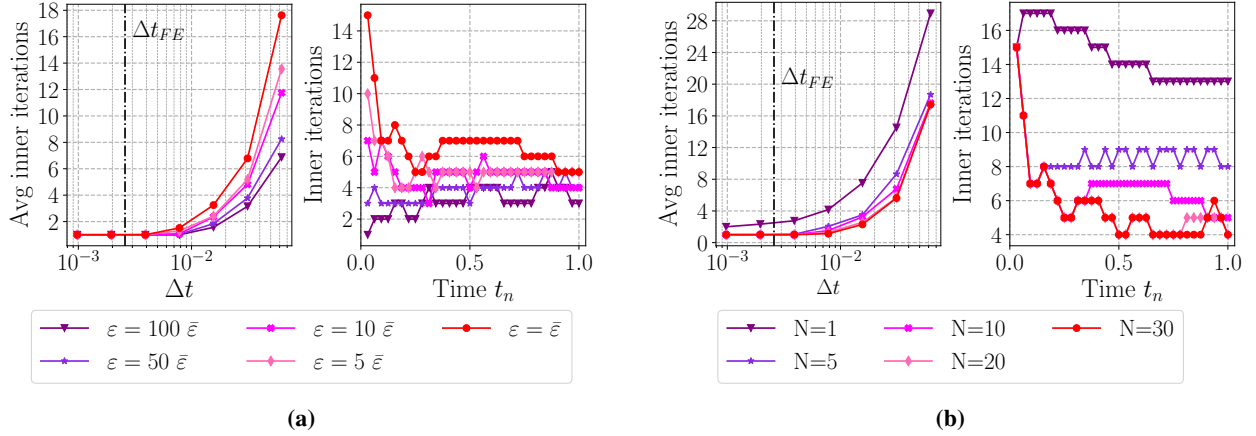


**Figure 7:** Study of the number of inner iterations performed by the IMEX–RB method, on the 3D advection–diffusion problem. We study how the average number of inner iteration varies when for different values of  $\Delta t$ , and the trend of iterations over time for  $\Delta t = 1/32$ . (a) Varying the values of the absolute stability parameter  $\epsilon$ ; (b) varying the reduced basis initial size  $N$ . All the tests were conducted setting  $N_1 = N_2 = N_3 = 81$  and a maximal number of inner iterations  $M = 100$ . When varying  $\epsilon$ , we fix  $N = 10$ ; when varying  $N$ , we fix  $\epsilon = \bar{\epsilon}$ .

efficient: for  $\Delta t > \Delta t_{FE}$ , and  $h = 0.012$ , IMEX–RB requires half as much the computational time of the BE scheme. As already observed in the 2D scenario, a sweet spot enables IMEX–RB to achieve the fastest computational times for values of  $\Delta t > \Delta t_{FE}$ , but not too large. Indeed, for the largest values of  $\Delta t$ , IMEX–RB performs too many inner iterations, thus hindering computational efficiency.

Further insights are provided by Figure 7a, which analyzes the scenario  $h = 0.012$  in more detail. Here, the smaller the imposed value of  $\epsilon$ , the larger the number of inner iterations that must be performed to meet the absolute stability criterion of Eq. (11). This explains the increasing CPU times for decreasing values of  $\epsilon$  for  $\Delta t > \Delta t_{FE}$ . The trend of average number of inner iterations varying  $\Delta t$  also shows that, for  $\Delta t \lesssim \Delta t_{FE}$ , one inner iteration suffices to guarantee absolute stability for all different thresholds  $\epsilon$ . This is because, as  $\Delta t \rightarrow 0$ ,  $\mathbf{u}_n \rightarrow \mathbf{u}_{n+1}$ ; the initial subspace at timestep  $n + 1$  already almost contains  $\mathbf{u}_{n+1}$ . Hence, the inequality of Eq. (11) is more easily satisfied.

The average number of inner iterations also grows when employing smaller values of the initial basis size  $N$  (Figure 7b). As expected, this behavior is mitigated when employing smaller values of  $\Delta t$ . Moreover, for values of  $N \geq 5$ , the number of inner iterations remains comparable, both when averaging over varying  $\Delta t$  values and when fixing  $\Delta t = 1/32$  and examining their evolution over time. In the latter case, while for the initial timesteps some 15 to 10 iterations are performed, for the following timesteps IMEX–RB always performs around 8 iterations ( $N = 5$ ) and 4 iterations ( $N = 30$ ).

The CPU times reported in Figure 6b show that the difference in terms of inner iterations does not justify employing  $N$  greater than 5: no further improvement in computational efficiency is noticed. Additionally, the convergence study of Figure 6b confirms that the achieved accuracy is, by construction of the method, independent of  $N$ , as long as the absolute stability criterion is met. In particular, for all values of  $\Delta t$  considered, the error made by the IMEX–RB scheme overlaps that of BE, and order 1 convergence is observed.

## 4 Conclusion

In this paper, we propose a first–order accurate IMEX–RB time integration. The method is proven to be convergent and unconditionally stable through both analytical derivations and numerical validation, enabling high–fidelity results even for time step sizes exceeding the stability threshold of the forward Euler method. The method’s hyperparameters — namely, the stability tolerance and the reduced basis dimension — play a critical role in its performance.

Stability is guaranteed when the tolerance is chosen in accordance with the theoretically derived upper bound of Eq. (12). Although this bound is often overly conservative, it can be effectively relaxed in practice for linear problems by selecting a value of the stability tolerance proportional to the inverse of the system matrix’s condition number, as demonstrated in our numerical experiments.

The reduced basis dimension must be selected by the user based on the specific problem, striking a balance between satisfying the absolute stability condition and minimizing computational and memory costs. In all our numerical

experiments, the dimension of the reduced basis is chosen to be significantly smaller than the number of DOFs, which ensures a low computational cost while keeping the storage requirements for the high–fidelity solution modest.

It is possible to identify a range of time step sizes — exceeding the stability limit of the explicit Euler method — within which IMEX–RB yields substantial computational advantages over backward Euler. The extent of this range is problem–dependent and is influenced by both the size of the reduced basis and the number of DOFs of the full–order system. In particular, our 3D test cases suggest a strong correlation between the efficiency gains of IMEX–RB and the increasing number of DOFs, highlighting the method’s scalability in high–dimensional settings.

Ongoing and future work aims to extend the proposed IMEX–RB framework by leveraging the well–established class of IMEX schemes based on Runge–Kutta methods to develop higher–order variants. Another important direction involves incorporating mass matrices into the underlying ODE systems, which would enable the application of IMEX–RB to PDEs discretized in space using Finite Element Methods (FEM) or other schemes where a mass matrix naturally arises in the semi–discrete formulation. Furthermore, we plan to extend the methodology to more challenging and computationally intensive problems, such as the Navier–Stokes equations, the two–fluid turbulence plasma model [10], and gyrokinetic simulations. The associated high–dimensional systems, characterized by stiff dynamics and complex interactions, present ideal scenarios where the efficiency and adaptability of IMEX–RB could be particularly advantageous. Finally, an additional line of research concerns domain decomposition, where a specific treatment of the mass matrix could lead to improved computational performance and better scalability in parallel computing environments.

## Acknowledgements

This work was supported by the *Swiss National Science Foundation* (grant agreement No 200021\_197021, “Data–driven approximation of hemodynamics by combined reduced order modeling and deep neural networks”).

## Code availability

The underlying code for this study is currently not available, but may be provided to qualified researchers upon request. Future publications of the software are planned to support transparency and reproducibility.

## References

- [1] J.D. Lambert. *Numerical Methods for Ordinary Differential Systems: The Initial Value Problem*. John Wiley and Sons, 1991.
- [2] D.F. Griffiths and D.J. Higham. *Numerical Methods for Ordinary Differential Equations: Initial Value Problems*. Springer Undergraduate Mathematics Series. Springer London, 2010. ISBN: 9780857291486.
- [3] Richard Courant, Kurt Friedrichs, and Hans Lewy. “Über die partiellen Differenzgleichungen der mathematischen Physik”. In: *Mathematische annalen* 100.1 (1928), pp. 32–74.
- [4] Dale R Durran. *Numerical methods for wave equations in geophysical fluid dynamics*. Vol. 32. Springer Science & Business Media, 1998.
- [5] Willem Hundsdorfer and Jan G Verwer. *Numerical solution of time–dependent advection–diffusion–reaction equations*. Vol. 33. Springer Science & Business Media, 2013.
- [6] Uri M Ascher, Steven J Ruuth, and Brian TR Wetton. “Implicit–explicit methods for time–dependent partial differential equations”. In: *SIAM Journal on Numerical Analysis* 32.3 (1995), pp. 797–823.
- [7] Uri M Ascher, Steven J Ruuth, and Raymond J Spiteri. “Implicit–explicit Runge–Kutta methods for time–dependent partial differential equations”. In: *Applied Numerical Mathematics* 25.2–3 (1997), pp. 151–167.
- [8] E Hofer. “A partially implicit method for large stiff systems of ODEs with only few equations introducing small time–constants”. In: *SIAM Journal on Numerical Analysis* 13.5 (1976), pp. 645–663.
- [9] Christopher A Kennedy and Mark H Carpenter. “Additive Runge–Kutta schemes for convection–diffusion–reaction equations”. In: *Applied numerical mathematics* 44.1–2 (2003), pp. 139–181.
- [10] S. I. Braginskii. “Transport Processes in a Plasma”. In: *Reviews of Plasma Physics* 1 (Jan. 1965), p. 205.
- [11] Hauke Doerk and Frank Jenko. “Towards optimal explicit time–stepping schemes for the gyrokinetic equations”. In: *Computer Physics Communications* 185.7 (2014), pp. 1938–1946.
- [12] Adam Preuss, Jessica Lipoth, and Raymond J Spiteri. “When and how to split? A comparison of two IMEX splitting techniques for solving advection–diffusion–reaction equations”. In: *Journal of Computational and Applied Mathematics* 414 (2022), p. 114418.

- [13] Vu Thai Luan and Alexander Ostermann. “Exponential Rosenbrock methods of order five–construction, analysis and numerical comparisons”. In: *Journal of Computational and Applied Mathematics* 255 (2014), pp. 417–431.
- [14] Alfio Quarteroni, Andrea Manzoni, and Federico Negri. *Reduced basis methods for partial differential equations: an introduction*. Vol. 92. Springer, 2015.
- [15] Jan S Hesthaven, Gianluigi Rozza, Benjamin Stamm, et al. *Certified reduced basis methods for parametrized partial differential equations*. Vol. 590. Springer, 2016.
- [16] Karl Kunisch and Stefan Volkwein. “Galerkin proper orthogonal decomposition methods for parabolic problems”. In: *Numerische mathematik* 90 (2001), pp. 117–148.
- [17] Karl Kunisch and Stefan Volkwein. “Galerkin proper orthogonal decomposition methods for a general equation in fluid dynamics”. In: *SIAM Journal on Numerical analysis* 40.2 (2002), pp. 492–515.
- [18] Peter Binev et al. “Convergence rates for greedy algorithms in reduced basis methods”. In: *SIAM journal on mathematical analysis* 43.3 (2011), pp. 1457–1472.
- [19] Annalisa Buffa et al. “A priori convergence of the greedy algorithm for the parametrized reduced basis method”. In: *ESAIM: Mathematical modelling and numerical analysis* 46.3 (2012), pp. 595–603.
- [20] Ngoc-Cuong Nguyen, Gianluigi Rozza, and Anthony T Patera. “Reduced basis approximation and a posteriori error estimation for the time–dependent viscous Burgers’ equation”. In: *Calcolo* 46.3 (2009), pp. 157–185.
- [21] Masayuki Yano. “A space–time Petrov–Galerkin certified reduced basis method: Application to the Boussinesq equations”. In: *SIAM Journal on Scientific Computing* 36.1 (2014), A232–A266.
- [22] Youngsoo Choi and Kevin Carlberg. “Space–time least–squares Petrov–Galerkin projection for nonlinear model reduction”. In: *SIAM Journal on Scientific Computing* 41.1 (2019), A26–A58.
- [23] Jan S Hesthaven, Cecilia Pagliantini, and Gianluigi Rozza. “Reduced basis methods for time–dependent problems”. In: *Acta Numerica* 31 (2022), pp. 265–345.
- [24] Riccardo Tenderini, Nicholas Mueller, and Simone Deparis. “Space–time reduced basis methods for parametrized unsteady Stokes equations”. In: *SIAM Journal on Scientific Computing* 46.1 (2024), B1–B32.
- [25] Allan Pinkus. *N–widths in Approximation Theory*. Vol. 7. Springer Science & Business Media, 2012.
- [26] Othmar Koch and Christian Lubich. “Dynamical low–rank approximation”. In: *SIAM Journal on Matrix Analysis and Applications* 29.2 (2007), pp. 434–454.
- [27] Abram Rodgers and Daniele Venturi. “Step–truncation integrators for evolution equations on low–rank tensor manifolds”. In: *CoRR* (2020).
- [28] Emil Kieri and Bart Vandereycken. “Projection methods for dynamical low–rank approximation of high–dimensional problems”. In: *Computational Methods in Applied Mathematics* 19.1 (2019), pp. 73–92.
- [29] Gianluca Ceruti and Christian Lubich. “An unconventional robust integrator for dynamical low–rank approximation”. In: *BIT Numerical Mathematics* 62.1 (2022), pp. 23–44.
- [30] Gianluca Ceruti, Jonas Kusch, and Christian Lubich. “A rank–adaptive robust integrator for dynamical low–rank approximation”. In: *BIT Numerical Mathematics* 62.4 (2022), pp. 1149–1174.
- [31] Joseph Nakao, Jing-Mei Qiu, and Lukas Einkemmer. “Reduced Augmentation Implicit Low–rank (RAIL) integrators for advection–diffusion and Fokker–Planck models”. In: *SIAM Journal on Scientific Computing* 47.2 (2025), A1145–A1169.
- [32] A. Quarteroni, F. Saleri, and P. Gervasio. *Scientific Computing with MATLAB and Octave*. Texts in Computational Science and Engineering. Springer Berlin Heidelberg, 2010. ISBN: 9783642124303.
- [33] A. Quarteroni, R. Sacco, and F. Saleri. *Numerical Mathematics*. Texts in Applied Mathematics. Springer Berlin Heidelberg, 2006. ISBN: 9783540346586.
- [34] James W Daniel et al. “Reorthogonalization and stable algorithms for updating the Gram–Schmidt QR factorization”. In: *Mathematics of Computation* 30.136 (1976), pp. 772–795.
- [35] Gene H. Golub and Charles F. van Loan. *Matrix Computations*. Fourth. JHU Press, 2013. ISBN: 9781421407944.
- [36] Randall J. LeVeque. *Finite Difference Methods for Ordinary and Partial Differential Equations*. Society for Industrial and Applied Mathematics, 2007.
- [37] Youcef Saad and Martin H Schultz. “GMRES: A generalized minimal residual algorithm for solving nonsymmetric linear systems”. In: *SIAM Journal on scientific and statistical computing* 7.3 (1986), pp. 856–869.
- [38] A.Refik Bahadır. “A fully implicit finite–difference scheme for two–dimensional Burgers’ equations”. In: *Applied Mathematics and Computation* 137.1 (2003), pp. 131–137. ISSN: 0096-3003.
- [39] Xiaojia Yang, Yongbin Ge, and Bin Lan. “A class of compact finite difference schemes for solving the 2D and 3D Burgers’ equations”. In: *Mathematics and Computers in Simulation* 185 (2021), pp. 510–534. ISSN: 0378-4754.